Mon. Not. R. Astron. Soc. **000**, 1–23 (0000) Printed 2 February 2008 (MN LATEX style file v1.4)

On the source of the late-time infrared luminosity of SN 1998S and other type II supernovae

M. Pozzo[1], W.P.S. Meikle[1], A. Fassia[1], T. Geballe[2], P. Lundqvist[3], N.N. Chugai[4] and J. Sollerman[3]

[1] *Imperial College London, Blackett Laboratory, Prince Consort Road, London, SW7 2BW, UK*
[2] *Gemini Observatory, 670 N. A'ohoku Place, Hilo, HI 96720, USA*
[3] *Stockholm Observatory, AlbaNova, Dept. of Astronomy, Stockholm SE 106 91, Sweden*
[4] *Insitute of Astronomy, RAS, Pyatnitskaya 48, 109017, Russia*

Accepted ... . Received .... ; in original form 2004 March 2

ABSTRACT

We present late-time near-infrared (NIR) and optical observations of the type IIn SN 1998S. The NIR photometry spans 333–1242 days after explosion, while the NIR and optical spectra cover 333–1191 days and 305–1093 days respectively. The NIR photometry extends to the M'-band (4.7 μm), making SN 1998S only the second ever supernova for which such a long IR wavelength has been detected. The shape and evolution of the Hα and He I 1.083 μm line profiles indicate a powerful interaction with a progenitor wind, as well as providing evidence of dust condensation within the ejecta. The latest optical spectrum suggests that the wind had been flowing for at least 430 years. The intensity and rise of the HK continuum towards longer wavelengths together with the relatively bright L' and M' magnitudes shows that the NIR emission was due to hot dust newly-formed in the ejecta and/or pre-existing dust in the progenitor circumstellar medium (CSM). The NIR spectral energy distribution (SED) at about 1 year is well-described by a single-temperature blackbody spectrum at about 1200 K. The temperature declines over subsequent epochs. After $\sim$2 years the blackbody matches are less successful, probably indicating an increasing range of temperatures in the emission regions. Fits to the SEDs achieved with blackbodies weighted with λ^{-1} or λ^{-2} emissivity are almost always less successful. Possible origins for the NIR emission are considered. Significant radioactive heating of ejecta dust is ruled out, as is shock/X-ray-precursor heating of CSM dust. More plausible sources are (a) an IR-echo from CSM dust driven by the UV/optical peak luminosity, and (b) emission from newly-condensed dust which formed within a cool, dense shell produced by the ejecta shock/CSM interaction. We argue that the evidence favours the condensing dust hypothesis, although an IR-echo is not ruled out. Within the condensing-dust scenario, the IR luminosity indicates the presence of at least 10^{-3} M$_\odot$ of dust in the ejecta, and probably considerably more. Finally, we show that the late-time $(K-L')_0$ evolution of type II supernovae may provide a useful tool for determining the presence or absence of a massive CSM around their progenitor stars.

Key words: supernovae: individual: SN 1998S - supernovae: general - infrared: stars - circumstellar matter - dust - winds

1 INTRODUCTION

One of the challenges of supernova research is to obtain evidence about the nature and environment of the progenitor. Type IIn supernovae (SNe IIn) are so-called because of the presence of narrow lines in the spectra, originating in a relatively undisturbed circumstellar medium (CSM) (Schlegel 1990). The progenitors must therefore have undergone one or more mass-loss phases before explosion. By using the interaction of the supernova explosion with the resulting CSM we can obtain clues about the nature of the progenitor.

The study of SNe IIn may also help us to understand the origin of dust in the universe. More than 30 years ago, it was suggested (Cernuschi, Marsicano & Kimel 1965; Cernuschi, Marsicano & Codina 1967; Hoyle & Wickramasinghe

1970) that supernovae could be important sources of interstellar dust. More recent studies of the origins of grains (Gehrz 1989; Tielens 1990; Dwek 1998; Todini & Ferrara 2001; Nozawa et al. 2003) still invoke core-collapse SNe as significant contributors of dust to the interstellar medium in the past and present. Dust grains associated with SNe can be detected both via their attenuation effects on optical/near-IR radiation, and by their thermal re-radiation at longer IR wavelengths of the absorbed energy. Observation of attenuation provides a relatively unambiguous way of demonstrating grain condensation in the ejecta. This process is revealed by the relative suppression of the red wings of the broad spectral lines. However, apart from SN 1998S (Leonard et al. 2000; Gerardy et al. 2000; this work), only for two events, SN 1987A and SN 1999em, has the condensation of dust in the ejecta been demonstrated via the attenuation of the red wing of the line profiles (Danziger et al. 1991; Lucy, Danziger & Gouiffes 1989; Lucy et al. 1991; Elmhamdi et al. 2003).

The second method of demonstrating grain condensation via the appearance of strong IR radiation (an 'IR excess') as a supernova ages, is more challenging. At least 10 SNe have shown a strong, late-time (i.e. $t > 100$ d) NIR excess (relative to that expected by extrapolation from the optical region; see references in Gerardy et al. 2002). The natural interpretation is that this radiation is produced by hot dust. However, while such grains may be the result of condensation processes in the expanding SN ejecta, they may also have formed in pre-explosion circumstellar material ejected during one or more mass-loss episodes experienced by the progenitor star. In this latter case, the IR emission is produced as an "IR echo" of the maximum-light luminosity from the CSM dust. Thus, in the interpretation of such strong NIR emission from SNe, a key issue is the location of the source. Only in the case of SN 1987A has conclusive evidence for dust condensation in the ejecta been presented on the basis of the NIR and mid-IR emission (Moseley et al. 1989; Whitelock et al. 1989; Suntzeff & Bouchet 1990; Dwek 1991; Lucy et al. 1991; Dwek et al. 1992; Meikle et al. 1993; Roche, Aitken & Smith 1993; Colgan et al. 1994). Recently, Dunne et al. (2003) have presented evidence based on sub-mm observations that $\sim 2-4\ M_{\odot}$ of cold dust is present in the supernova remnant (SNR) Cassiopeia A. They argue that the dust must have been produced during the explosion. A similar result for the Kepler SNR was presented by Morgan et al. (2003) although in this case an alternative CSM origin for the dust was not ruled out, which would be more consistent with the most commonly believed origin for this supernova, i.e. a type Ia explosion. Such sub-mm studies may provide important support for the hypothesis that supernovae are a major source of dust. However, at the moment they have the disadvantages that the supernova types are uncertain, and that the number of examples which can be studied in this way is quite small. In addition, the results of Dunne et al. (2003) and Morgan et al. (2003) have been criticised by Dwek (2004) who points out that, given the mass of condensible elements expected in the ejecta, a very unlikely condensation efficiency of 100% would be required to yield even 2 $M_{\odot}$ of dust. Moreover thermal sputtering would reduce this mass of dust. Dwek offers an alternative scenario where the sub-mm emission is from conductive needles ("metallic whiskers") which may be long enough to be very efficient emitters at sub-mm wavelengths thus requiring a dust mass of no more than 10^{-3} $M_{\odot}$ to account for the observed radiation.

Lastly, we note that the unique wavelength and temporal coverage of SN 1987A also made it possible to infer dust condensation from (a) spectroscopic evidence for the temporal depletion of gaseous-phase elements in the ejecta e.g., [O I] (6300, 6364 Å), [Mg I] (4571 Å), Si I (1.2 μm), [Si I] (1.65 μm) and [Ca II] (7300 Å) (Lucy et al. 1991; Spyromilio et al. 1991; Meikle et al. 1993), and (b) analysis of the luminosity budget of the ejecta (e.g. Whitelock et al. 1989). As observing facilities improve, these last two methods of dust detection may eventually be applicable to SNe at more typical distances.

To provide conclusive evidence of SNe as major dust sources, we need to assemble a statistically significant sample of typed supernovae in which grain formation can be reliably tested. In addition, by studying the evolution of recent supernovae in real time we can obtain information about the physics of the dust-formation process. In order to disentangle the two possible origins of the NIR radiation, it is vital to acquire IR observations spanning as wide a wavelength and temporal range as possible. The longer NIR wavelengths ($HKLM$ bands) are especially important since the flux at these wavelengths is less likely to be contaminated by scattered light or strong H, He emission lines, allowing a simple thermal interpretation.

An opportunity to address both the progenitor problem and the question of supernovae as dust sources was provided by the occurrence of the SN IIn 1998S. This is the most intensively-studied type IIn event (Bowen et al. 2000; Fassia et al. 2000, 2001; Gerardy et al. 2000, 2002; Leonard et al. 2000; Lentz et al. 2001; Liu et al. 2000; Roscherr & Schaefer 2000; Anupama, Sivarani & Pandey 2001; Chugai 2001; Wang et al. 2001; Chugai et al. 2002; Gruendl et al. 2002; Li et al. 2002; Pooley et al. 2002; Meikle et al. 2003).

1.1 SN 1998S at early epochs

SN 1998S is one of the brightest SN IIn ever seen, reaching $V = +12.17$ on 1998 March 18 (Fassia et al. 2000). It was discovered by Z. Wan (Li & Wan 1998) on 1998 March 2.68 UT (JD 2,450,875.18) in NGC 3877, an edge-on Sc spiral galaxy. The supernova lies about 16" west and 46" south of the galaxy nucleus (see Fig. 1). It was identified as a SN IIn by Filippenko & Moran (1998). Liu et al. (2000) point out that the BV light curves together with the spectroscopic behaviour at 2–3 months are similar to those of the type IIL SN 1979C. Hamuy (2003) suggests that SNe IIn are actually a subset of what he terms "dense wind" type II supernovae which includes SN 1979C. A pre-discovery limiting magnitude of $\sim$+18 obtained on 1998 February 23.7 (Leonard et al. 2000) indicates that SN 1998S was discovered within a few days of shock breakout. Following Chugai (2001) we adopt 1998 February 24.7 UT = JD 2,450,869.2, 6 days prior to discovery, as the explosion epoch, $t = 0$ days. Relative to this epoch, the zero epochs adopted by other authors are later by, respectively, +5 days (Leonard et al. 2000), +6 days (Fassia et al. 2000, 2001; Pooley et al. 2002), $\sim$+23 days (Bowen

Figure 1. A J-band image (83" × 83") showing SN 1998S (centre) at 333 days after shock breakout. North is to the top and east to the left. The image was obtained with the United Kingdom Infrared Telescope, Hawaii.

et al. 2000; Gerardy et al. 2000, 2002). Throughout this paper, epochs quoted from other authors have been shifted to our zero epoch definition. We adopt a distance of 17 Mpc (Tully 1988), but note that a smaller value of 15.5 Mpc is sometimes adopted (Sanders & Verheijen 1998; Gerardy et al. 2002).

The earliest optical spectra of SN 1998S show a blue continuum with emission features superimposed. A rough blackbody fit yields T∼25,000 K, but with a blue excess (Leonard et al. 2000; Fassia et al. 2001). The emission lines are identified with H I (Balmer series), He I, He II, C III and N III. The high-ionisation carbon and nitrogen lines are also commonly observed in Wolf-Rayet stars (Leonard et al. 2000). The emission lines have a broad base (e.g., Hα FWZI∼20,000 km s^{-1}), but a narrow 'peaked' unresolved centre. The lines are symmetrical about the local standard of rest. This is quite surprising since at such an early phase most of the receding part of the supernova should be occulted by the photosphere. However, this may actually constitute some of the earliest evidence of a strong ejecta-CSM wind interaction. It has been shown theoretically that, at this phase, one might expect the photosphere to reside in a geometrically thin, opaque cool dense shell (CDS) formed by the radiative shock propagating into the extended stellar envelope (Grasberg, Imshennik & Nadyozhin 1971; Falk & Arnett 1977; Chevalier & Fransson 1985; 1994). Chugai (2001) has argued that these lines originate from the CDS and that the line broadening is caused by the multiple Thomson scattering of line photons on thermal electrons of the circumstellar gas. The weakness of broad ejecta lines during this early era is attributed to the sharp photosphere at the SN ejecta boundary. The blue excess can also be attributed to the CDS, since the significant optical depth can yield an increase in continuum absorptive opacity with wavelength, due to both bound-free, (i.e., the Paschen continuum) and

free-free processes (Leonard et al. 2000).

By about 3 weeks after the explosion, the emission lines had almost totally vanished. This disappearance is attributed to the dense inner-CSM being overrun by the ejecta. This persisted for ∼3–7 weeks. During this time weak narrow lines are present, superimposed on the continuum. These are caused by the photoionization and heating of the undisturbed wind by the supernova flash and subsequent X-ray emission from the shocked wind and ejecta. High-resolution echelle spectra of these lines were obtained by Bowen et al. (2000) and Fassia et al. (2001) on days 23 and 42. These observations succeeded in resolving the lines. Between day 23 and day 42 the red wing of the [O III] 5007 Å profile moved redward, broadening the line, so that by the latter epoch the profile was symmetrical about a velocity of +847 km s^{-1}. A high-resolution observation of Gruendl et al. (2002) at 1 year showed that the [O III] 5007 Å profile was still symmetrical about this redshift. This behaviour can be explained as being due to the effect of the finite light travel time across a CSM having a denser outer zone. As the radiation-induced ionisation (due to the flash + shock radiation) propagates across the CSM, it takes longer for the resulting nebular emission to reach us from the far side. At any given time, therefore, the observer sees radiation from an ellipsoidal surface propagating through the CSM (Morrison & Sartori 1969). On day 23, the vertex region of the ellipsoid had not yet reached the inner boundary of the denser zone, thus accounting for the weakness of the red wing of the line. However, the lack of any further shift in the line centre between 46 days and 1 year indicates that the vertex had already reached the dense zone by 46 days. The early evolution of the line asymmetry can be quantitatively explained if the inner boundary of the denser zone was at a distance of 16.5 light days (2850 AU). We note that this distance is consistent with the observed persistence of the line for at least a year since, assuming a maximum ejecta velocity of 10,000 km s^{-1} (Leonard et al. 2000; Fassia et al. 2001), at 1 year it would still only have reached 2050 AU and so would not yet have disturbed the dense outer CSM region (but see subsection 4.2 below). Fassia et al. (2001) adopted +847 km s^{-1} as the centre of mass velocity for the SN 1998S system. Justification for this is provided by the light travel time argument together with the lack of any further shift between day 46 and 1 year. From the narrow forbidden lines such as [O III] 5007 Å, an undisturbed CSM velocity of about 40 km s^{-1} is obtained, which is characteristic of a red supergiant (RSG) wind. From the intensity ratio of [O III] (4959 Å + 5007 Å) to [O III] 4363 Å, Fassia et al. (2001) infer a CSM density of at least 1.5×10^6 cm^{-3} at 185 AU, implying a CSM mass exceeding 0.005 M$_\odot$, and a mass-loss rate exceeding around 2×10^{-5} M$_\odot$ yr^{-1}. This is consistent with the radio/X-ray estimate (scaled to a 40 km s^{-1} wind velocity) of $\sim 5 \times 10^{-4}$ M$_\odot$ yr^{-1} (Pooley et al. 2002), and is comparable to that of SN 1979C which had a mass loss rate of $\sim 1.2 \times 10^{-4}$ M$_\odot$ yr^{-1} (Lundqvist & Fransson 1988) .

The behaviour of the narrow allowed H I, He I CSM lines was more complex. Not only did they exhibit asymmetric P Cygni profiles, but there were clearly two velocity components. The slower component is attributed to the same origin as the forbidden lines *viz.* the photo-ionised, unaccelerated CSM. The profile of this component was probably a combination of emission from recombination and possibly collisional excitation, together with a classical P Cygni line due to scattering from the populated excited levels. The broad absorption component is more difficult to explain. It extends to a velocity of around 350 km s^{-1} which is too fast for a RSG wind. It may be that, as in the case of SN 1987A, the SN 1998S progenitor went through a fast-wind phase prior to explosion (Fassia et al. 2001). An alternative explanation is that the CSM close to the supernova was accelerated by photospheric photons, or by relativistic particles from the ejecta/CSM shock (Chugai et al. 2002). Another possibility is that the faster component arose in shocked clumps within the CSM wind (Chugai et al. 2002). By day 50, broad emission lines in Pβ and He I 1.083 μm had appeared. The earliest second season optical spectra (day 78) showed a similar development in Hα and the Ca II triplet (Fassia et al. 2001). The line profiles became increasingly "square-shaped", characteristic of strong interaction between the expanding ejecta and a dense CSM (Leonard et al. 2000; Fassia et al. 2000). This was confirmed by the detection of radio and X-ray emission (Pooley et al. 2002) plus an unusually slow decline in V and I by ∼300 days (Li et al. 2002).

In summary, the wind of the SN 1998S progenitor underwent discrete changes in the rate of mass outflow, resulting in several distinct CSM zones. The fading of the early-time broad emission components by about day 18 indicates that the radius of the first boundary was less than 100 AU (Leonard et al. 2000; Fassia et al. 2001). Beyond this boundary the density presumably fell quite sharply. The later appearance of broad emission features led Leonard et al. (2000) and Fassia et al. (2001) to suggest the presence of a second boundary where the CSM underwent a density increase. For the explosion epoch adopted here, the reappearance occurred between days 42 and 50 corresponding to 260 ± 20 AU. However, the reality of this second boundary was contested by Chugai et al. (2002) who suggested the reappearance was due simply to the CDS becoming optically thin. Finally, as argued above, the evolution of the narrow-line profile suggests a third boundary at about 2850 AU where the CSM again underwent a density increase. For a wind velocity of 40 km s^{-1}, these three boundaries correspond to material which left the progenitor at epochs −12 yr, −30 yr and −340 yr relative to the explosion date. Pooley et al. (2002) also note that the best fit to their radio data requires significant clumping or filamentation in the CSM, a condition already inferred in two other type II SNe, 1986J and 1988Z. Early-time spectropolarimetry by Leonard et al. (2000) and Wang et al. (2001) indicate asphericity in the ejecta, CSM or possibly both.

SN 1998S is unique in that it allowed the first-ever good IR spectroscopic coverage of a SN IIn (Gerardy et al. 2000; Fassia et al. 2001). In the J-band, we see Paschen β, Paschen γ and He I 1.083 μm lines. Their evolution was similar to that seen in the optical. At the earliest times broad-based, peaked profiles were present. These faded by day 23, being replaced by broad, square-shaped profiles by day 50. Between days ∼15 and ∼60 a strong, unresolved He I 1.083 μm CSM line was superimposed on the ejecta/CSM broad lines. By day 50, the HK-band was dom-

inated by Paschen α. By day 114, first-overtone CO emission was clearly present in the K-band. The presence of CO in type II SNe is increasingly regarded as ubiquitous. In all cases where K-band observations have been carried out in the period 3-6 months post-explosion, CO has been detected, e.g., SN 1987A (IIpec) (Catchpole & Glass, 1987; McGregor & Hyland, 1987; Spyromilio et al. 1988; Meikle et al. 1993), SN 1995ad (IIP) (Spyromilio & Leibundgut 1996), SN 1998S (IIn) (Gerardy et al. 2000; Fassia et al. 2001), SN 1999dl (IIP) (Spyromilio, Leibundgut & Gilmozzi 2001), SN 1999em (IIP) (Spyromilio et al. 2001; Gerardy et al. 2002), SN 1999gi (IIP) (Gerardy et al. 2002) and SN 2002hh (IIP) (Pozzo et al., in preparation). In addition, CO has been detected in the type Ic SN 2000ew (Gerardy et al. 2002). The rotation-vibration states of CO are a powerful coolant (especially the fundamental band lines). The presence of CO is suspected to be a necessary condition for dust condensation to occur in the ejecta. Modelling of the SN 1998S spectra suggests a CO velocity of $\sim$2000 km s^{-1} (Gerardy et al. 2000; Fassia et al. 2001). From this, Fassia et al. (2001) deduced a core mass of 4 M$_\odot$ implying a massive progenitor. The actual mass of CO derived was 10^{-3} M$_\odot$. This is much smaller than the > 0.1 M$_\odot$ of C and > 1.0 M$_\odot$ of O likely to be present in the ejecta (Woosley & Weaver 1995), implying that most of the C and O remain in the gas phase and are thus available to condense into, respectively, graphite and silicate grains.

On day 136, Fassia et al. (2000) measured the IR flux out to a wavelength of 3.8 μm (L'-band). This revealed a remarkable IR excess of $K - L' = +2.5$. To produce the observed flux the lowest possible radius of the IR emission region is given by a blackbody with a temperature close to the dust evaporation temperature of $\sim$1500 K. For dust condensing in the ejecta to attain a sufficiently large blackbody radius by 136 days would require an expansion velocity of 11,000 km s^{-1} (see Fassia et al. 2000). Such high velocities were seen only in the extreme outer zones of the H/He envelope. No metals were seen at such high velocities. Fassia et al. (2000) concluded that the IR excess at this epoch cannot, therefore, have been due to grain condensation in the ejecta. It must instead have been produced by an IR echo of the maximum-light luminosity from pre-existing dust in the CSM. This conclusion is based only on the intensity of the L'-band flux. It is strengthened if we fit a blackbody to both the K and L' fluxes. After correction for the optical photosphere, this yields $K - L' \approx 3.7$ corresponding to a temperature of only 650 K, requiring the dust to lie at an equivalent velocity of at least 67,000 km s^{-1}!

SN 1998S was exceptionally luminous, reaching a dereddened $M_B = -19.6$ (Fassia et al. 2000). This is around $\times$10 the typical luminosity of a type II SN. The excellent early-time coverage achieved in the optical and NIR allowed Fassia et al. (2000) to examine the bolometric light curve. Both blackbody and UVOIR (i.e., ultraviolet-optical-infrared range) fits indicate that the total energy radiated in the first 40 days exceeded 10^{50} ergs, which is again $\times$10 the typical value for type II SNe. Between days 96 and 136, the bolometric light curve is well-reproduced by the radioactive decay luminosity of 0.15 M$_\odot$ ^{56}Ni. However, by this era the ejecta/CSM shock energy must also have been making a contribution.

1.2 SN 1998S at later epochs

Much of the early-time behaviour of SN 1998S can be attributed to the interaction of the supernova with a pre-existing, dusty, perhaps disk-like CSM. SN 1998S remained observable from X-rays to radio for over 3 years (Pooley et al. 2002; this work) due to the ongoing conversion of the SN kinetic energy to radiation via the ejecta/CSM interaction. We continued regular observations during this phase, to day 1242. A brief, preliminary presentation of this work was given in Meikle et al. (2003). Other late-time studies have been presented: optical spectroscopy to 499 d (Leonard et al. 2000); high-resolution spectroscopy at $\sim$ 370 d (Gruendl et al. 2002); NIR spectroscopy to $\sim$ 380 d and NIR photometry to 819 d (Gerardy et al. 2000, 2002); X-ray observations to 1055 d and radio observations to 1065 d (Pooley et al. 2002).

In this paper we present and discuss NIR photometry of SN 1998S spanning 333 to 1242 days post-explosion, optical spectra covering 305 to 1093 days and IR spectra covering 333 to 1191 days. The NIR photometry presented here extends as far as the M'-band (CW 4.7 μm), the first time that such a long IR wavelength has been detected in any SN other than the exceptionally close SN 1987A. The paper is organised as follows. NIR photometry and optical/NIR spectroscopy are presented in Section 2. The evolution of the Hα and He I 1.083 μm profiles are examined in detail, and for this purpose the data are augmented by spectra from other sources. In Section 3 we compare the NIR spectral energy distribution (SED) with pure blackbody functions and blackbodies weighted by emissivities λ^{-1} and λ^{-2}. In Section 4 we examine possible energy sources for the post-300 d NIR emission, and discuss the location of the IR-emitting dust. Evidence of episodic mass-loss from the progenitor is discussed. We also compare the late-time $(K - L')_0$ colour evolution of SN 1998S with that of other type II SNe and suggest that it provides a useful identifier of supernovae whose progenitors had a massive CSM. Conclusions follow in Section 5.

2 OBSERVATIONS

2.1 Near-infrared photometry

$JHKL'M'$ images of SN 1998S were obtained in the period 333-1242d at the 3.8m United Kingdom Infrared Telescope (UKIRT) on Mauna Kea (Hawaii). The NIR observations for the earlier epochs were obtained with the IRCAM3 camera. This contains a 256×256 InSb array, originally with a 0.286 arcsec/pixel plate scale. In late 1999, the camera was reconfigured to a plate scale of 0.081 arcsec/pixel, and renamed TUFTI. Also during 1999, a new camera, UFTI, was introduced. This contains a 1024×1024 HgCdTe array with a 0.091 arcsec/pixel scale. Most of the later JHK images were obtained with UFTI, with the L' and M' images being taken with TUFTI (see Table 1 for details). IRCAM3 used the older J(Barr), H(Barr), K(OCLI), L'(OCLI) and nbM

Table 1. Log of infrared imaging of SN 1998S at UKIRT

JD(2450000+)	Date	Epoch[a]	Filters[b]	Standard star[c]
1202.2	1999 Jan 23	333.0	J, H, K, L'	FS21, HD105601
1243.2	1999 Mar 3	374.0	J, H, L', nb$M$	FS15, HD84800, HD105601, HD106965
1274.8	1999 Apr 4	405.5	$J98$, $H98$, $K98$	FS21
1333.5	1999 Jun 2	464.2	J, H, K, L', nb$M$	FS21, HD106965
1533.2	1999 Dec 19	664.0	$J98$, $H98$, $K98$, $L'98$, $M'98$	FS130, HD105601
1567.5	2000 Jan 23	698.2	$J98$, $H98$, $K98$, $L'98$, $M'98$	FS21, HD105601
1579.0	2000 Feb 4	709.8	$M'98$	HD105601
1696.2	2000 May 30	827.0	$J98$, $H98$, $K98$, $L'98$, $M'98$	FS21, HD105601
1916.8	2001 Jan 7	1047.5	$J98$, $H98$, $K98$, $L'98$, $M'98$	FS21, HD105601, HD106965
2067.0	2001 Jun 5	1197.8	$J98$, $H98$, $K98$	FS131
2111.5	2001 Jul 19	1242.2	$L'98$	HD106965

[a] Days after explosion, assumed to be 1998 February 24.7 UT (JD 2450869.2).
[b] See subsection 2.1 for details.
[c] FS standards were used for JHK, and HD standards for $L'M'$.

Table 2. Infrared photometry of SN 1998S

JD(2450000+)	Epoch[a]	J	H	K	L'	M'
1202.2	333.0	16.653(12)[b]	14.809(5)	13.344(2)	11.560(28)	–
1243.2	374.0	16.799(34)	14.922(13)	–	11.52(17)	11.291(86)
1274.8	405.5	17.077(25)	15.269(8)	13.431(2)	–	–
1333.5	464.2	17.609(29)	15.537(12)	13.806(4)	11.69(13)	11.14(16)
1533.2	664.0	18.025(33)	16.421(14)	14.448(4)	11.856(18)	11.44(14)
1567.5	698.2	18.341(35)	16.728(15)	14.556(4)	11.970(26)	11.82(14)
1579.0	709.8	–	–	–	–	12.30(12)
1696.2	827.0	18.680(27)	17.148(16)	14.992(4)	12.200(33)	$> 11.9(2\sigma)$[c]
1916.8	1047.5	19.280(48)	17.956(27)	15.843(7)	12.985(39)	12.84(15)
2067.0	1197.8	19.798(83)	18.439(77)	16.366(13)	[13.29(3)][d]	–
2111.5	1242.2	–	–	[16.52(2)][e]	13.40(15)	–

[a] Days after explosion.
[b] Figures in brackets give the statistical error, in units of the magnitude's least significant one or two digits.
[c] For this epoch we did not detect the SN in the M' filter band image.
[d] Estimated by linear interpolation within L'-band light curve.
[e] Estimated by linear extrapolation of K-band light curve.

filters at effective central wavelengths of 1.25, 1.65, 2.205, 3.8 and 4.675 μm; UFTI/TUFTI uses the newer Mauna Kea Filter set $J98$(MK), $H98$(MK), $K98$(MK), $L'98$(MK) and $M'98$(MK) at effective wavelengths of 1.25, 1.635, 2.20, 3.77 and 4.68 μm (see Tokunaga, Simons & Vacca 2002). For JHK, UKIRT faint standard stars were observed, while for $L'M'$ we used HD standards. Table 1 lists the log of the observations plus information on the different filter sets and UKIRT standards. 5-point and 9-point dither patterns were used in the JHK and $L'M'$ filter bands respectively.

The images were reduced using the standard Starlink packages IRCAMDR (Aspin 1996) and ORAC-DR (Economou et al. 2003). Magnitudes were measured via aperture photometry within the Starlink package GAIA* (Draper, Gray & Berry 2002). The sky background was measured using a concentric annular aperture. Choice of target aperture and sky annulus was a compromise between maximising the S/N, and minimising the effects of the galaxy background gradients and structure. An aperture radius of 1.4 arcsec was selected, this being equivalent to 5 pixels for IRCAM3, 15.4 pixels for UFTI and 17.3 pixels for TUFTI. The annulus was set to cover $\times 3$ the area of the target aperture in order to minimise the effect of statistical uncertainty in the background estimation (Merline & Howell 1995). Thus, the annulus was chosen to have inner and outer radii, respectively, $\times 1.5$ and $\times 2.5$ that of the aperture. Statistical uncertainty in the photometry was determined by the sky variance method, with 2 sigma clipping rejection (all points in the sky background measurement which deviate by more than 2 standard deviations from the mean are rejected). Magnitudes were determined by comparison with the standard stars listed in Table 1. Systematic uncertainties arising from varying atmospheric conditions from epoch to epoch or between the target and standard are discussed in Section 3.

The $JHKL'M'$ magnitudes for SN 1998S are listed in Table 2 together with associated statistical errors in parentheses. The quoted errors do not include additional uncertainty due to differences in conditions under which the supernova and standards were observed. The light curves are

* Graphical Astronomy and Image Analysis Tool, version 2.6-9

Table 3. Infrared colours of SN 1998S

JD(2450000+)	Epoch (days)	$J-H$	$H-K$	$K-L'$	$L'-M'$
1202.2	333.0	1.844(13)[a]	1.465(5)	1.784(28)	–
1243.2	374.0	1.877(36)	–	–	0.23(19)
1274.8	405.5	1.808(26)	1.838(8)	–	–
1333.5	464.2	2.072(31)	1.731(13)	2.11(13)	0.55(20)
1533.2	664.0	1.604(36)	1.973(15)	2.592(18)	0.41(14)
1567.5	698.2	1.613(38)	2.172(16)	2.586(26)	0.15(14)
1696.2	827.0	1.532(31)	2.156(16)	2.792(33)	–
1916.8	1047.5	1.324(55)	2.113(28)	2.858(40)	0.15(15)
2067.0	1197.8	1.36(11)	2.073(78)	[3.08(3)][b] –	–
2111.5	1242.2	–	–	[3.12(15)][c] –	–

[a] Figures in brackets give the statistical error, in units of the magnitude's least significant one or two digits.
[b] Estimated by linear interpolation within L'-band light curve.
[c] Estimated by linear extrapolation of K-band light curve.

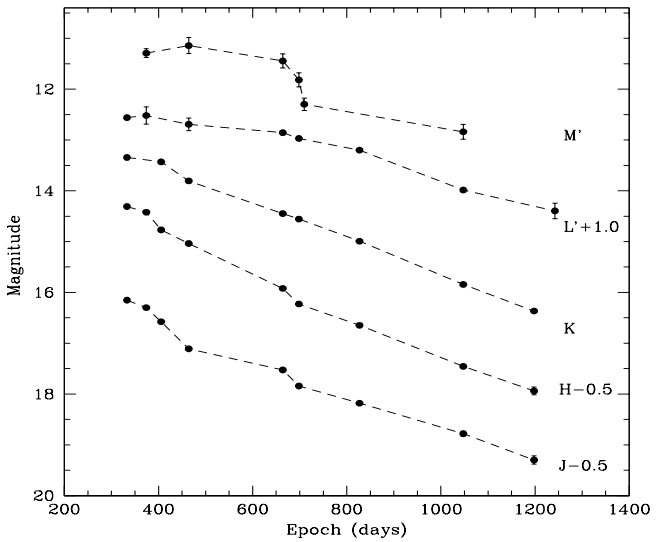

Figure 2. Post-300 d $JHKL'M'$ light curves of SN 1998S. Only the statistical errors are shown (see text).

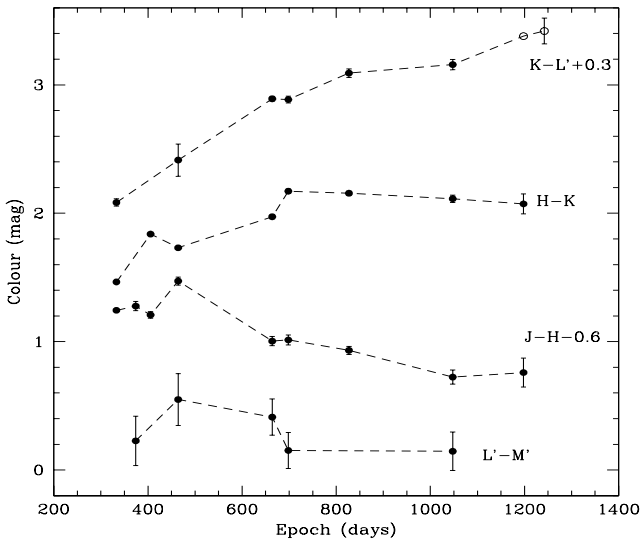

Figure 3. Post-300 d IR colour evolution of SN 1998S. The latest two $K-L'$ values (open circles) were estimated by linear interpolation between L'-band values (penultimate point) or linear extrapolation of the K-band values (final point). Only the statistical errors are shown (see text).

shown in Fig. 2. They extend to longer wavelengths and to later phases than has ever been achieved for the IR light curves of any supernova other than SN 1987A. A generally monotonic decline is seen in the $JHKL'$ bands. The M'-band light curve shows a sudden fading of about 1 mag. at around 700 days, although the errrors are quite large.

The NIR colours for each epoch are listed in Table 3, and their evolution is illustrated in Fig. 3. We note in particular the increase in $H-K$ to day$\sim$700 d and in $K-L'$ to beyond 1000 d. The latter reached a value of 2.9 by 1047 d. Indeed, using modest linear extrapolation of the K-band magnitudes we see that by 1242 d, $K-L'$ has reached a value of 3.1.

2.2 Spectroscopy

We obtained optical spectroscopy at the Nordic Optical Telescope (NOT) and the Isaac Newton Telescope (INT), both on La Palma. Infrared spectroscopy was obtained at the United Kingdom Infrared Telescope (UKIRT), Hawaii. Tables 4 and 5 give the observing logs of the optical and IR observations respectively. For the IR spectroscopy, the standard BS4431 was used.

The day 1093 NOT spectra, the INT spectrum and the UKIRT spectra were reduced using the standard routines of the FIGARO package (Shortridge 1991). The other NOT spectra were reduced using the standard procedures within IRAF.† The fluxing of the day 1093 NOT spectrum was corrected using contemporary photometry in a narrow band Hα filter (CW 6556 Å, width 162 Å). The Hα image is shown in Fig. 4 together with a contemporary V-band image. The source of the Hα emission is clearly visible as a point source

† IRAF(Image Reduction and Analysis Facility) is distributed by the National Optical Astronomy Observatory (NOAO), which is operated by the Association of Universities for Research in Astronomy (AURA), Inc. under cooperative agreement with the National Science Foundation.

Table 4. Log of optical spectroscopy of SN 1998S

JD[a]	Date (UT)	Epoch (d)	Telescope/ Instrument	Spectral range (Å)	Spectral res. (Å)	Slit width (arcsec)	Spectrophotometric standard
1174.5	1998 Dec. 27	305.3	NOT/ALFOSC	5825-8344	3.0	1.2	G191b2b
1215.6	1999 Feb. 6.1	346.4	INT/IDS	4350-7700	5.0	1.2	Feige 34
1287.5	1999 Apr. 19	418.3	NOT/ALFOSC	5100-9095	8.4	1.3	Feige 34
1343.5	1999 Jun. 14	474.3	NOT/ALFOSC	5804-8322	3.0	1.3	Feige 56
1962.6	2001 Feb. 22.1	1093.4	NOT/ALFOSC	4000-8500	8.3	1.3	Feige 34
"	"	"	"	5802-8340	3.0	"	"

[a] 2450000+

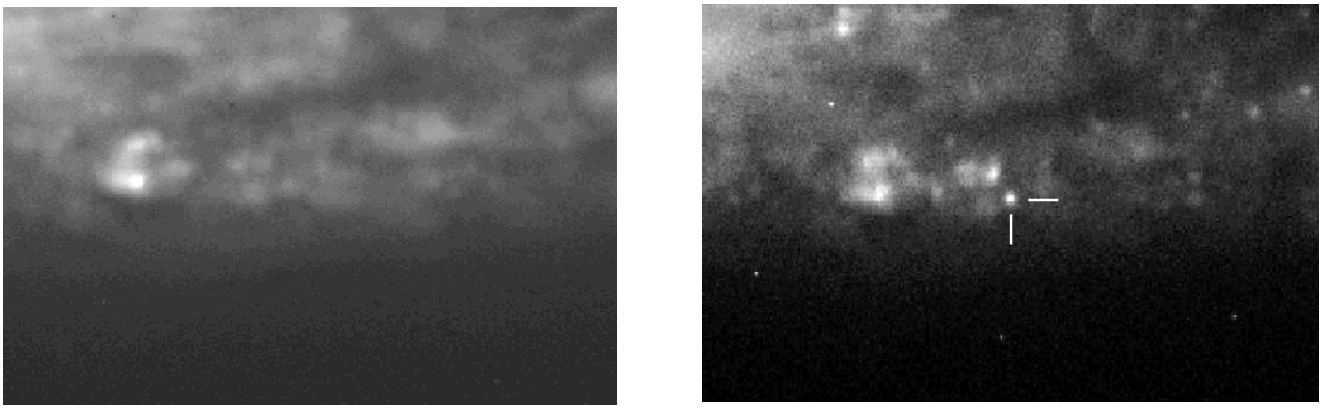

Figure 4. V-band (left hand image) and Hα (right hand image) images of SN 1998S taken with ALFOSC at the Nordic Optical Telescope at 1093 days post-explosion. North is approximately towards the top left-hand corner. The images cover 69 arcsec. × 42 arcsec.

Table 5. Log of UKIRT/CGS4 infrared spectroscopy of SN 1998S

JD[a]	Date (UT)	Epoch (d)	Spectral range (μm)	Spectral res. ($10^{-4}\mu$m)	Slit width (arcsec)
1203.0	1999 Jan. 24.5	333.8	1.01-1.33	12.5	0.61
			1.45-2.51	25	0.61
1228.1	1999 Feb. 18.6	358.9	1.01-1.33	25	1.23
1273.1	1999 Apr. 4.6	403.9	1.01-1.33	25	1.23
1567.2	2000 Jan. 23.7	698.0	1.02-1.34	25	1.23
1578.1	2000 Feb. 3.6	708.9	1.02-1.34	25	1.23
			1.84-2.48	50	1.23
1918.2	2001 Jan. 8.7	1049.0	1.79-2.40	50	2.46
2060.8	2001 May 31.3	1191.6	1.03-1.35	25	1.23
			1.83-2.46	50	1.23

[a] 2450000+

in the Hα image. From these we obtain approximate magnitude estimates of: $V = 21.25 \pm 0.6$ and $m_{H\alpha} = 20.15 \pm 0.3$. A contemporary R-band image yields $R = 20.3 \pm 0.5$. The IR spectra fluxing was adjusted to match the IR photometry in Table 2. The spectra are plotted in Figs. 5, 6 (optical) and 7 (IR).

The optical spectra are dominated throughout by a broad, complex Hα profile. This is described in more detail below. At a much lower level, however, broad emission from a few other species can be identified (Fig. 6). Between days 305 and 474, we identify He I 5876 Å and [Ca II] 7291, 7324 Å. On day 418 the spectrum extends far enough to the red to reveal a blend of [O I] 8446 Å and [Ca II] 8498, 8542, 8662 Å. The He I feature exhibits a peak blueshifted by ∼–4000 km s^{-1}, as does the [O I] 8446 Å peak (assuming it dominates the blend with the calcium triplet). These blueshifts are similar to those seen in the Hα line peaks (see below). There is some evidence of a similarly blueshifted Hβ peak in the day 346 spectrum. In the same spectrum there may also be a [O III] 5007 Å peak blueshifted by about 3000 km s^{-1}. The [Ca II] 7291, 7324 Å line peak on days 305 and 418 shows a blueshift of only about 2300 km s^{-1}. Given the larger blueshifts seen in the other oxygen lines, this argues against a significant blended contribution from [O II] 7319, 7330 Å. The broad feature lying at 5100-5400 Å has been identified as an Fe II emission band (Garnavich, Challis & Kirshner 1998). On day 1093, we identify Hβ, He I 5876 Å, [O I] 6300 Å and [O III] 4363, 5007 Å. A fainter feature at about 7275 Å could be due to [O II] 7319, 7330 Å, possibly blended with [Ca II] 7291, 7324 Å. The profiles appear to have a similar form to that of Hα at this epoch, with much of the flux appearing as a broad feature to the blue of the local rest frame wavelengths. Narrow peaks at the rest wavelengths are also seen, although these may be simply unresolved emission from a coincident H II region. However, we

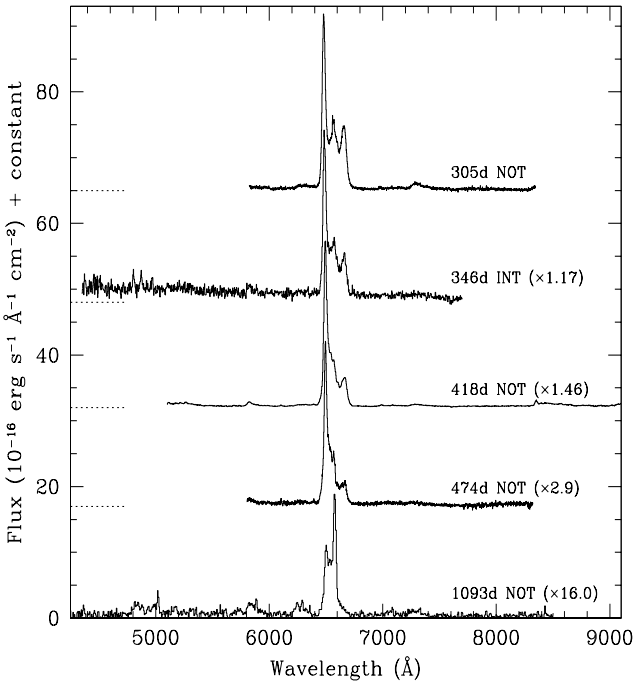

Figure 5. Post-300 d optical spectra of SN 1998S obtained with the IDS spectrograph at the Isaac Newton Telescope or with the ALFOSC spectrograph on the Nordic Optical Telescope, both on La Palma. The zero flux levels are shown by the horizontal dotted lines on the left-hand side. In addition, the spectral fluxes have been scaled by the factors shown in brackets. Throughout the period covered, the spectrum is dominated by Hα emission. For more detailed displays of these spectra see Figs. 6 (weaker lines) and 8 (Hα lines).

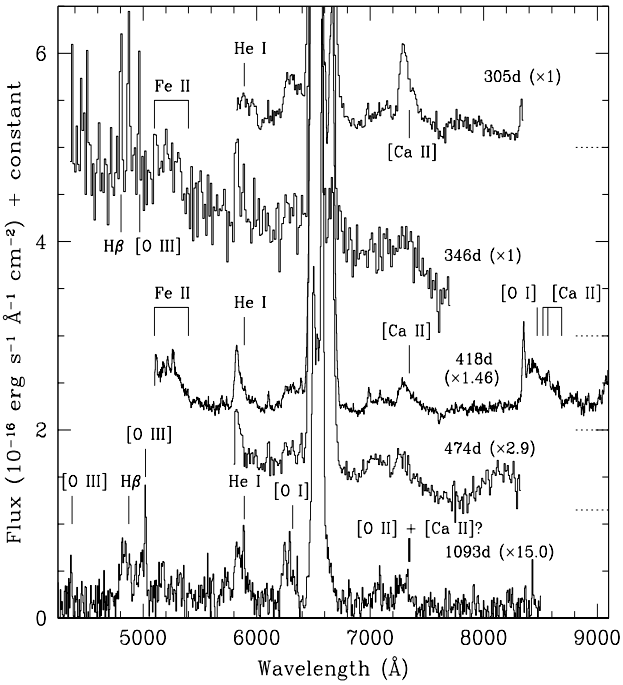

Figure 6. Post-300 d optical spectra of SN 1998S, plotted to show the weaker features. The line wavelengths in the SN 1998S restframe are usually indicated. The exception is in the day 346 spectrum where, for clarity, the blueshifted peaks of Hβ and [O III] 5007 Å are shown. The zero flux levels are shown by the horizontal dotted lines on the right-hand side. In addition, the spectral fluxes have been scaled by the factors shown in brackets.

note that a higher resolution spectrum of the much stronger Hα feature (Fig. 8) reveals a rest-frame peak with wings extending to $\pm$1000 km s^{-1}, making a H II region origin unlikely, at least for this line (see below).

The IR spectra are characterised by strong, broad complex He I 1.083 μm emission plus, when observed, a smooth continuum rising to longer wavelengths. Pα and Pβ are also visible in the day 333 spectrum.

2.2.1 Hα and He I 1.083 μm profiles

In Fig. 8 we show the evolution of the Hα profile between days 103 and 1093. To maximise the temporal coverage, we have added spectra at +103 d (Fassia et al. 2001), +249 d (Gerardy et al. 2000) and at +658 d (D. Leonard and T. Matheson, private communication). The +658 d spectrum was placed on an absolute flux scale by interpolation of the Hα intensity light curve which declined at about 1mag/155 days between days 249 and 1093. The velocities of the peaks and extreme edges of the profile with respect to the SN centre-of-mass velocity are listed in Table 6, together with the mean flux and intensity of the line.

On day 103 the profile has the form of a broad, steep-sided, fairly symmetrical line spanning $\pm$7000 km s^{-1} across the base. This appearance persisted to at least day 145 (Leonard et al. 2000). However, by the time the supernova was recovered in the second season, the shape was remarkably different. The day 249 spectrum of Gerardy et al. (2000) shows that the profile had developed a triple-peak structure, comprising a central peak close to the rest-frame velocity, and two outlying peaks at, respectively, –4860 km s^{-1} and +3400 km s^{-1}. Gerardy et al. suggest that the outermost peaks could have been produced by an emission zone having a ring or disk structure seen nearly edge-on, and resulting from the SN shock-wave collision with the disk/ring. Following Chugai & Danziger (1994) they also suggest that the central peak might have been due to shocked wind clouds. Between days 249 and 658 we see a steady fading of the central and red-shifted peaks with respect to the blue-shifted peak. Gerardy et al. (2000) and Leonard et al. (2000) also observed this effect, suggesting that dust condensation in the ejecta is responsible. We note also that the strong blue peak shifted from –4860 km s^{-1} on day 249 to –3900 km s^{-1} by day 474, presumably due to a slowing of the shock as it encountered an increasing mass of CSM. The velocity then remained fairly constant for the subsequent $\sim$200 d. Finally, when we recovered the supernova in the 4th season on day 1093, it can be seen that the profile had undergone another dramatic change. While the blue-shifted peak persisted, slowing slightly to –3430 km s^{-1}, the central peak had grown in relative strength to about twice the height of the blue peak. However, the total intensity of the day 1093

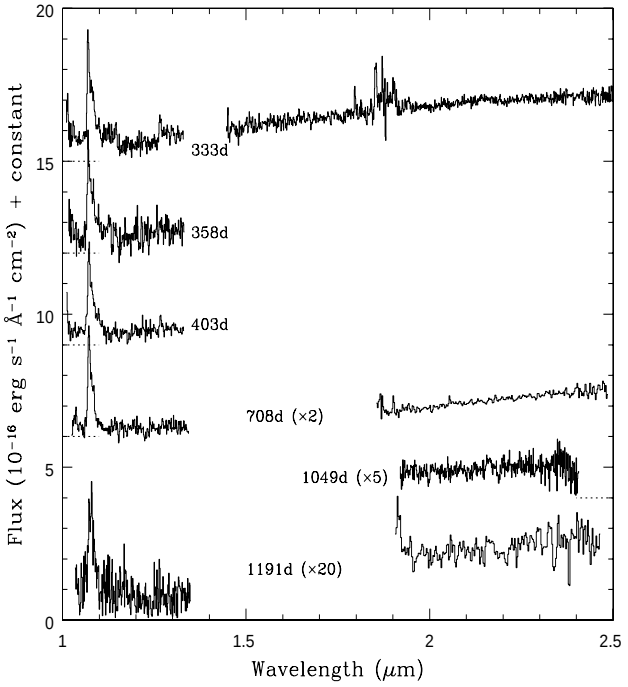

Figure 7. Post-300 d IR spectra of SN 1998S obtained with the CGS4 spectrograph on UKIRT, Hawaii. The spectra have been displaced vertically for clarity. The zero flux levels are shown by the horizontal dotted lines on the left-hand side or, for 1049 d, on the right. In addition, the spectral fluxes for the latest three epochs have been scaled by the factors shown in brackets. For a more detailed display of the He I 1.083 μm profiles see Fig. 9

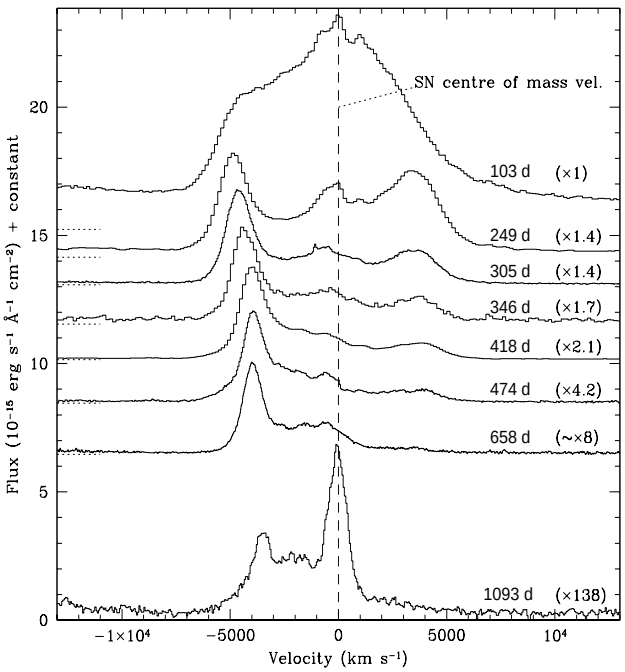

Figure 8. Evolution of the Hα profile, in velocity space. Zero velocity corresponds to the rest frame of the SN 1998S system (see text). The spectra have been scaled by the amounts shown in brackets, in order to approximately normalise to the height of the blue-shifted peak. They have also been displaced vertically for clarity. The zero flux levels are shown by the horizontal dotted lines on the left-hand side. The day 103 spectrum is from Fassia et al. (2001), the day 249 spectrum from Gerardy et al. (2000), and the day 658 spectrum from D. Leonard and T. Matheson (private communication). The day 658 spectrum was placed on an absolute flux scale by interpolation of the Hα intensity light curve.

line is less than 10% of the day 658 spectrum and so it is possible that the day 1093 central peak was present at earlier times but was swamped by other stronger emission.

In Fig. 9 we show a sequence of He I 1.083 μm spectra obtained at UKIRT. Again to increase the temporal coverage we include spectra obtained by Fassia et al. (2001) on day 114, and by Gerardy et al. (2000) on days 247 and 283. The velocities of the blue peak and extreme edges of the profile with respect to the SN centre-of-mass velocity are listed in Table 7, together with the mean flux and intensity of the line. Judging from the strength of Pβ emission, the earlier epochs were probably slightly contaminated by Pγ emission. Consequently the velocities of the red edges of the earlier epoch profiles are not well determined and the line intensity values are approximate. Although the signal-to-noise is lower, clearly the form and evolution of the strong He I 1.083 μm profile was similar to that of Hα.

3 COMPARISON OF THE IR SPECTRAL ENERGY DISTRIBUTION WITH THERMAL CONTINUA

The intensity and rise of the HK continuum towards longer wavelengths (Fig. 7) together with the relatively bright L' and M' magnitudes (Table 2) suggests strongly that the IR emission was due to hot dust condensing in the ejecta

Table 6. Evolution of the Hα line

Epoch (d)	Vel. (km s^{-1}) Blue Edge	Blue Peak	Mid-Peak	Red Peak	Red Edge	Flux[a]	I[b]
249	–7060	–4860	∼0	3400	∼7000	11.8	3.52
305.3	–6400	–4570	–560	3450	6050	8.4	2.30
346.4	–6120	–4340	–380	3770	5460	6.2	1.57
418.3	–6400	–3930	–650	3860	6050	4.3	1.17
474.3	–6260	–3890	–560	3950	5590	2.07	0.54
658	–5610	–3940	–550	3540	5270	(1.0)[c]	(0.25)
1093.4	–5760	–3430	–60	–	5460	0.10	0.027

[a] Mean Flux given in 10^{-16} erg s^{-1} cm^{-2} Å^{-1}.
[b] Intensity given in 10^{-13} erg s^{-1} cm^{-2}.
[c] Figures in brackets were estimated by interpolation

and/or pre-existing in the CSM. To investigate the location and hence origin of the dust, we fitted the IR $HKL'M'$ photometry flux values at each epoch (i.e. the IR SED), with single-temperature blackbodies. We excluded the J-band fluxes from the fits since these were probably dominated by emission from the ejecta gas (e.g. Pβ emission,

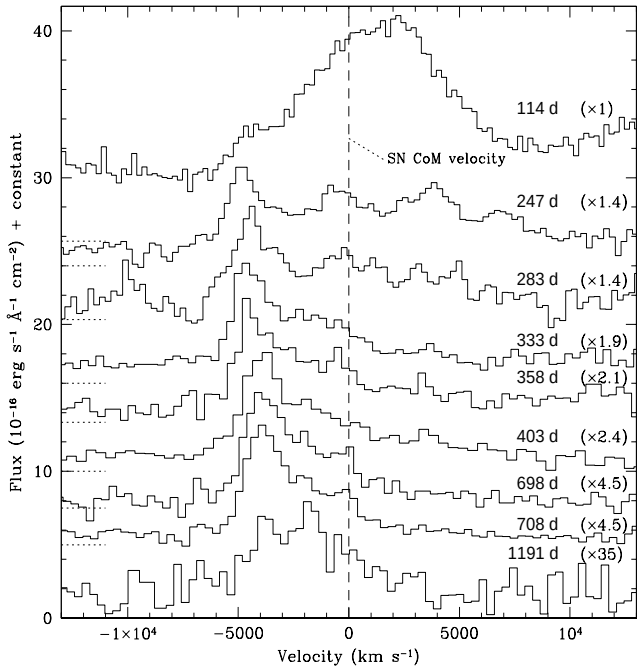

Figure 9. Evolution of the He I 1.083 μm profile, in velocity space. Zero velocity corresponds to the rest frame of the SN 1998S system (see text). The spectra have been scaled to show an approximately constant height in the blue-shifted peak. They have also been displaced vertically for clarity. The zero flux levels are shown by the horizontal dotted lines on the left-hand side. The 114 d spectrum is from Fassia et al. (2001) and the 247 d and 283 d spectra are from Gerardy et al. (2000).

residual photospheric emission) rather than hot dust (cf. Fig. 11). It is possible that the H-band might also have been slightly contaminated by non-dust emission. However, approximate extrapolation of the J-band continuum (Fig. 11) to longer wavelengths suggests that non-dust emission contributed less than ∼20% of the total flux in the H-band. The magnitudes for each waveband were dereddened using the empirical formula of Cardelli, Clayton & Mathis (1989) and adopting A_V=0.68 (Fassia et al. 2000). Using the effective wavelengths of the filters, the dereddened IR magnitudes were then converted into fluxes using the calibration curve of Bersanelli, Bouchet & Falomo (1991). Using χ^2 minimisation, blackbody fits to the IR fluxes at each epoch were then performed, with temperature T_{bb} and solid angle as free parameters. The errors used in the fits were not just the statistical errors given in Table 2, since these errors do not include systematic uncertainties arising from varying atmospheric conditions from epoch to epoch or between the target and standard. To obtain a more realistic assessment of the true error we note that, up to ∼800 days, the HKL' light curves declined approximately linearly (magnitudes v. time) but with an apparently random scatter in the measured values about this line. We assume that this scatter is due to the combination of statistical and systematic errors, rather than real fluctuations in the supernova decline. From the scatter we derive total uncertainties of at least ±0.05 magnitudes in HK, and ±0.06 in L'. Where the statistical errors are larger than this, then these were used. In the M'-band the relatively small number of points and the apparent sudden fading around 700 days (cf. Fig. 2) means that it is not possible to estimate the total error from the scatter. However, given that the statistical error alone is ±0.1 to ±0.15 mags, we adopt a total uncertainty of ±0.2 in M'. The fits were repeated using a blackbody scaled by λ^{-1} and λ^{-2} emissivity dependence such as might be the case for optically-thin emission.

Table 7. Evolution of the He I 1.083 μm line

Epoch (d)	Vel. (km s^{-1}) Blue Edge	Blue Peak	Red Edge	Flux[a]	I[b]
247[c]	-6760	-4790	–	∼22	∼10
283	-6120	-4380	–	∼20	∼8
333.8	-6370	-4520	–	∼13	∼5
358.9	-5180	-4440	4700	13	4.8
403.9	-5820	-3720	4710	12	4.5
698.0	-5040	-3860	4600	6.5	2.2
708.9	-5210	-3830	4510	5.9	2.1
1191.6	∼-5000	-1730	∼3500	1.0	0.25

[a] Mean Flux given in 10^{-17} erg s^{-1} cm^{-2} Å^{-1}.
[b] Intensity given in 10^{-14} erg s^{-1} cm^{-2}.
[c] The earlier epochs are slightly contaminated by Pγ emission and so the red edge is undetermined and the intensities are only approximate.

The fits for a pure blackbody and for λ^{-1} emissivity dependence are illustrated in Fig. 10. Details of the fits are given in Table 8. Column 1 gives the epoch, and column 2 gives the number of points used in the fit, together with the corresponding wavebands in brackets. The quality (χ^2_{red}) of these fits is listed in columns 3 (blackbody) and 4 (λ^{-1}). For days 333, 374 and 464, single-temperature blackbody functions provide excellent descriptions of the IR SED. From day 664 the quality of the fits becomes somewhat poorer. However, apart from 374 d, for all the epochs the λ^{-1} emissivity fits were somewhat less successful than those using a pure blackbody SED. The quality of fits with λ^{-2} dependence was even poorer. In Fig. 11 we compare the blackbody and λ^{-1} emissivity curves with the coeval IR spectra, when the wavelength coverage extended into the K-band. It can be seen that up to the end of year 2, the continua are well-represented by the both pure blackbody and λ^{-1}-weighted blackbody functions. However, as Gerardy et al. (2002) noted, H and K data alone are insufficient to distinguish between different emissivity laws. The pure blackbody fits indicate that the temperature declined from ∼1250 K to ∼950 K at the end of year 2, but then remained relatively constant during the following year [cf. Table 8, col. 5 and Fig. 12(b)]. This is reflected in the slowing of the reddening in $K - L'$ (Fig. 3). Not surprisingly, temperatures obtained from the λ^{-1} emissivity case are lower (Table 8, col. 6). The shape and characteristic temperature of the SED supports our earlier suspicion that the emission is produced by heated dust grains in and/or around SN 1998S. Similar conclusions were reached by Gerardy et al. (2000). However, our coverage to longer wavelengths allows us also to conclude that

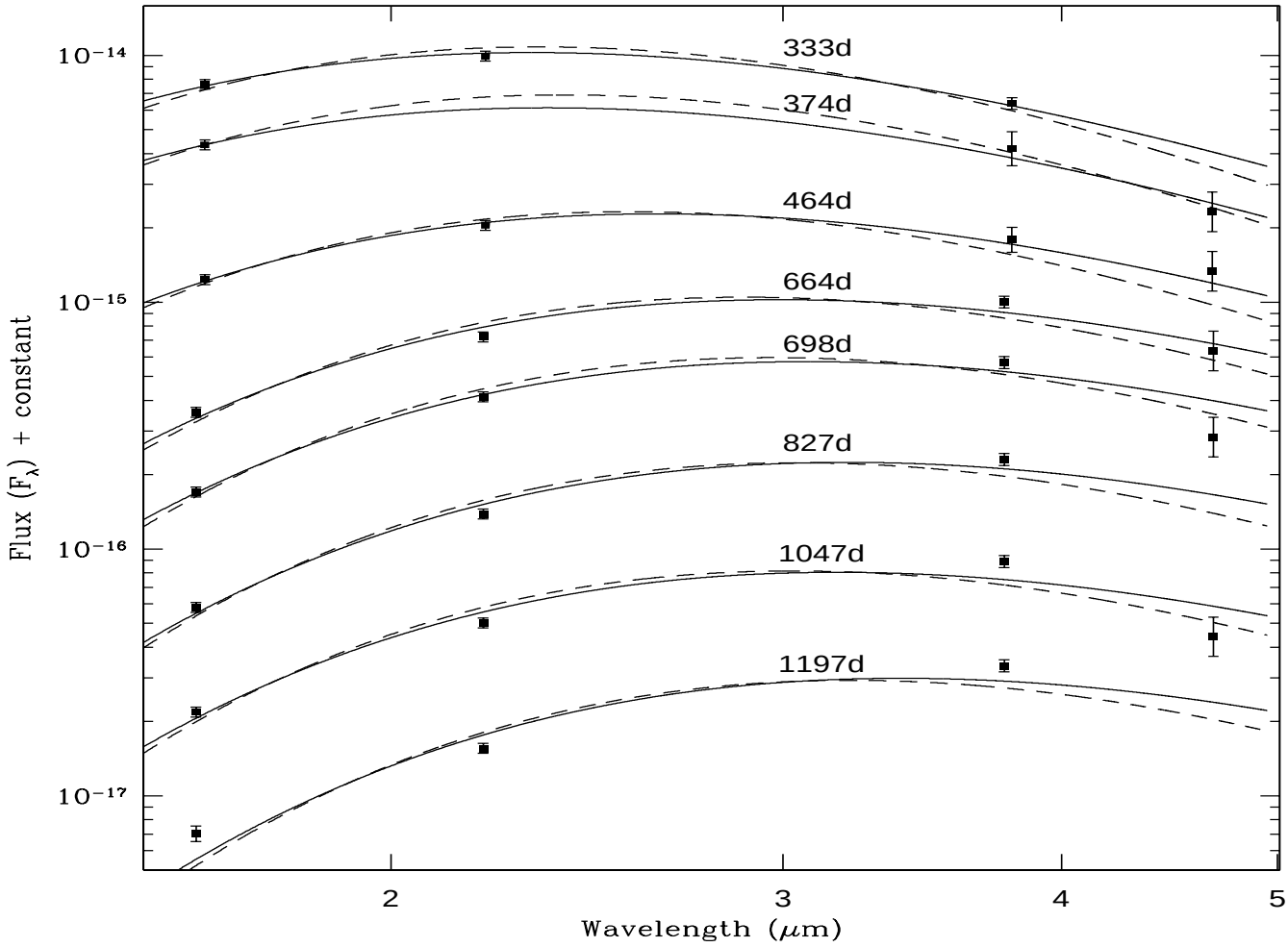

Figure 10. Blackbody (solid curves) and emissivity λ^{-1} fits (dashed curves) to $HKL'M'$ photometry of SN 1998S. The errors shown include statistical and estimated systematic errors (see text for details). The latest L'-band point was obtained by interpolation using the L' light curve. The observations are de-reddened, assuming $A_V = 0.68$ and the extinction law of Cardelli et al. (1989).

Table 8. Details of fits to the NIR SED of SN 1998S

Epoch (d)	npts(filters)[a]	χ^2_{red} [b] (bb)	χ^2_{red} [c] (λ^{-1})	T_{bb} [d] (K)	$T_{\lambda^{-1}}$ (K)	L_{bb} [e] (10^{41} erg s^{-1})	r_{bb} (10^{14} cm)	v_{bb} (km s^{-1})	L (^{56}Ni) [f] (10^{38} erg s^{-1})
333.0	3(HKL')	0.7	5.6	1254(23)[g]	1034(4)	2.51(8)	119(6)	4150(210)	995
374.0	3($HL'M'$)	0.5	0.1	1234(16)	1007(22)	2.42(11)	121(5)	3740(170)	689
464.2	4($HKL'M'$)	0.4	2.8	1102(22)	941(1)	2.01(12)	138(10)	3450(240)	307
664.0	4($HKL'M'$)	4.3	9.8	970(12)	836(5)	1.62(7)	161(7)	2800(130)	52.3
698.2	4($HKL'M'$)	3.6	4.5	943(10)	813(1)	1.49(6)	162(7)	2690(120)	38.7
827.0	3(HKL')	7.7	18.5	905(10)	792(7)	1.21(6)	159(7)	2220(100)	12.8
1047.5	4($HKL'M'$)	8.8	14.0	915(10)	795(7)	0.54(3)	104(5)	1150(50)	2.35
1197.8	3(HKL')	23	36.6	856(11)	749(7)	0.43(2)	106(6)	1020(60)	0.98

[a] Number of points used in the blackbody fits (corresponding wavebands as given in brackets).
[b] Reduced chi square values.
[c] These illustrate the poorer fits achieved with a λ^{-1}-weighted blackbody law.
[d] Fit parameters were derived after dereddening using Av=0.68 (Fassia et al. 2000) and the interstellar reddening law of Cardelli et al. (1989).
[e] The overall level of the luminosity light curve is subject to an additional uncertainty of about ±12% due to distance uncertainty (see text).
[f] Total power output of radioactive decay of 0.15 $M_\odot$ of ^{56}Ni (Li, McCray & Sunyaev 1994; Timmes et al. 1996; Fassia et al. 2000).
[g] Internal errors in last one or two significant figures are shown in brackets.

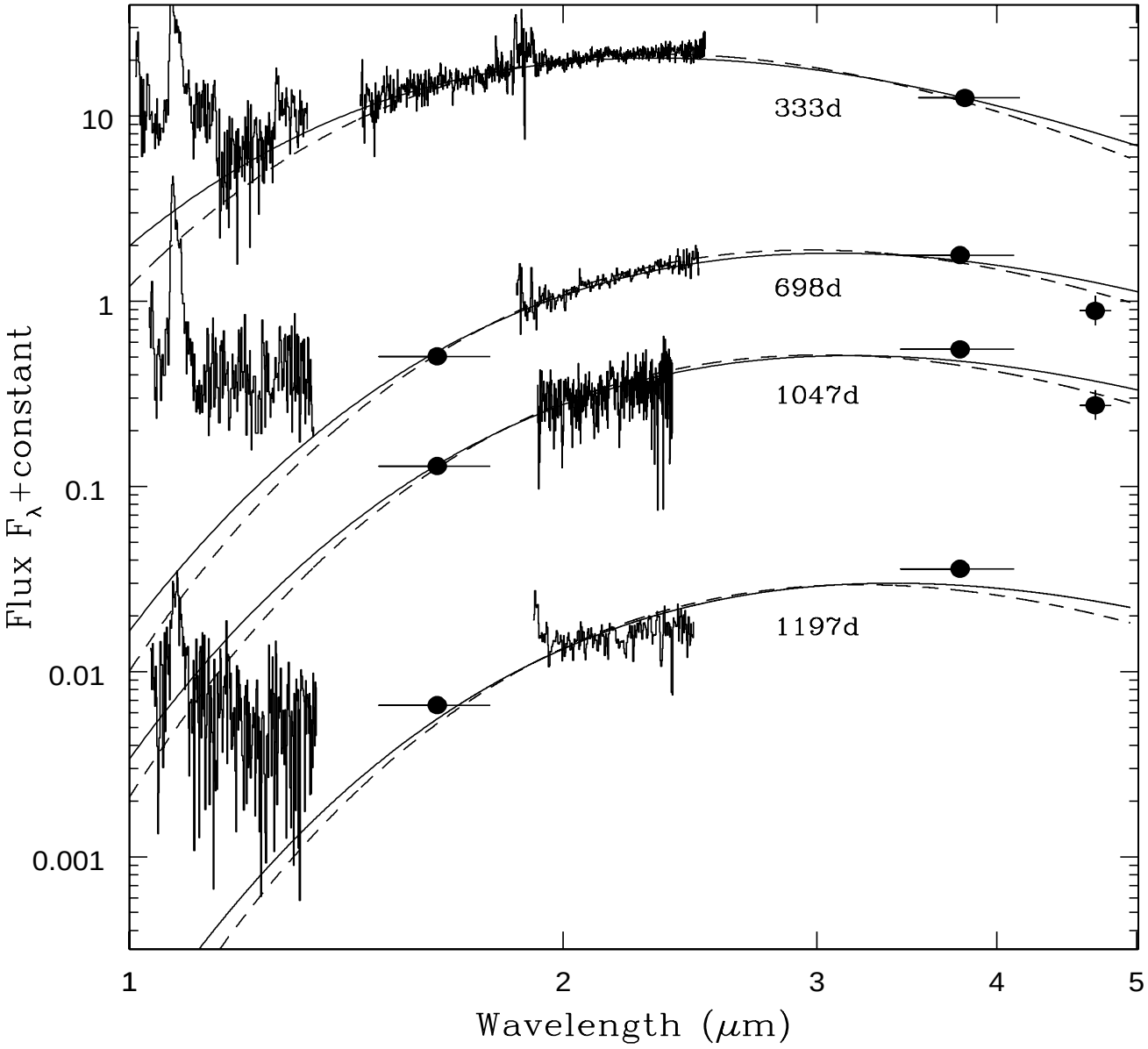

Figure 11. Comparison of blackbody (solid curves) and emissivity λ^{-1} fits (dashed curves) given in Figure 10, with contemporaneous IR spectra. Note that the fits did not include the J-band photometry since this wavelength region was probably dominated by emission from the ejecta gas rather than hot dust. [The lowest J-band spectrum corresponds to 1191 d (cf. Fig. 7) and so should be compared with the 1197 d fit]. Approximate extrapolation of the J-band continuum to longer wavelengths suggests that non-dust emission contributed less than ∼20% of the total flux in the H-band. Where no spectra are available, we show the H, L' and M' photometry values used in the fits (cf. Fig. 10). The horizontal bars on these points indicates the filter bandwidth (50% levels). The observations are de-reddened, assuming $A_V = 0.68$ and the extinction law of Cardelli et al. (1989).

pure blackbody fits appear somewhat superior.

Following a suggestion by the referee, we also examined fits using a λ^{+1} dependence, as might be the case if long iron whiskers can form in the SN ejecta (see Wickramasinghe 1992; Hoyle & Wickramasinghe 1999). We find that the quality of fits was generally no better than for blackbodies and so on this basis alone we do not rule out optically-thin emission with a λ^{+1} dependence. However, a problem with such emission is that it would require the condensing grains to be lying beyond the CDS. This is discussed further in Section 4.1.2.

Adopting a distance of 17 Mpc (Tully 1988) and an explosion date of 1998 February 24.7 (see subsection 1.1), we found the blackbody radius (r_{bb}) and velocity (v_{bb}) for each blackbody fit. Finally, we found the total flux and total luminosity (L_{bb}) by integrating the best-fit blackbody

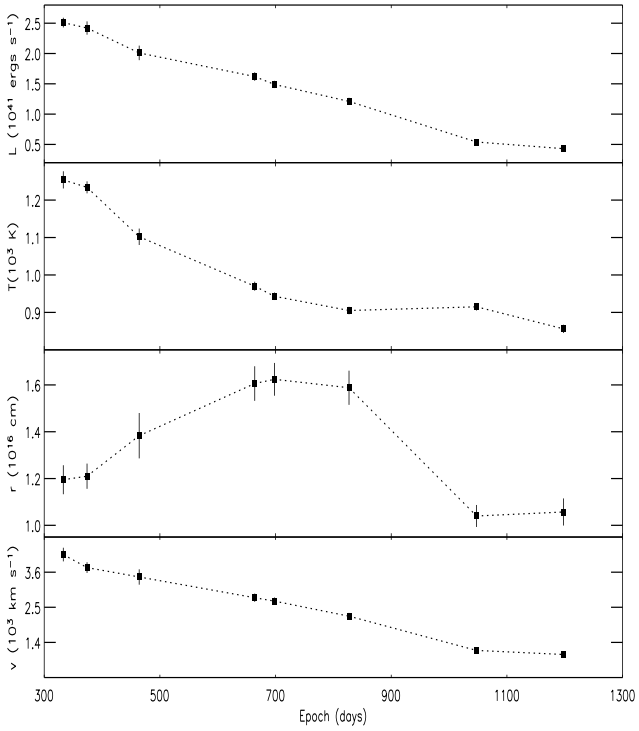

Figure 12. Evolution of the luminosity, temperature, radius and velocity derived from blackbody fits to the SN 1998S $HKL'M'$ magnitudes.

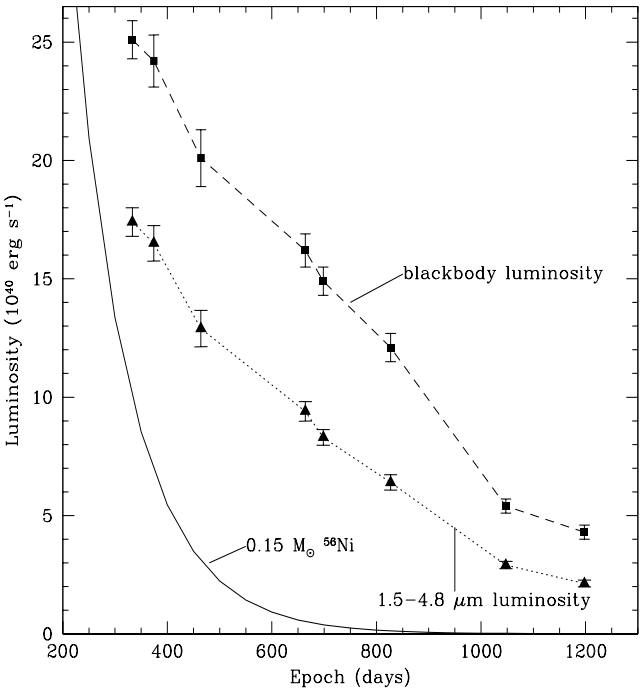

Figure 13. Evolution of the total power output due to the radioactive decay of 0.15 $M_\odot$ of ^{56}Ni (Fassia et al. 2000) compared with the IR luminosity obtained from (a) integrated blackbody fits (dashed line) and (b) blackbody fits integrated over the range 1.5–4.8 μm (dotted line).

curves. These values are listed in Table 8, cols. 7–9. and are plotted in Fig. 12(a,c,d). Throughout the 333–1197d era, the blackbody fits indicate a monotonically declining luminosity. The derived blackbody velocity declined monotonically from 4150 km s^{-1} on day 333 to 1020 km s^{-1} on day 1197, while the radius peaked at ∼1100 AU at about 2 years. Similar conclusions would be reached for grey-body emission (e.g. clumps of dust), except that the radii and velocities would be proportionally higher. For the λ^{-1} and λ^{-2} emissivity fits, similar trends with time are obtained, but with much larger velocities being required to account for the observed luminosity. The uncertainty in the extinction is quite large ($A_V = 0.68^{+0.34}_{-0.25}$, Fassia et al. 2000). Therefore, to check the effect on the above results, we repeated the fitting procedure using the range of A_V values encompassed by the errors. We conclude that the extinction uncertainty introduces an additional error of only 1% or 2% in the derived parameters.

As indicated in Section 1.1, there is some uncertainty about the distance to NGC 3877 at the level of about ±1 Mpc. Consequently this introduces an additional uncertainty of about ±12%. While this does not affect the shape of the bolometric luminosity light curve, it does act on its overall level.

4 DISCUSSION

4.1 Origin of the IR emission and location of the dust

What powered the post-300 d IR emission from the dust, and where was the dust located? Integrating over the single temperature blackbody fits, the total energy emitted by the dust region between days 300 and 1200 was about 10^{49} ergs, or 0.6×10^{49} ergs in the 1.5-4.8 μm range. Even for the more conservative value, this is a factor of ×50 more than could be supplied by the decay of the daughter products of 0.15 $M_\odot$ ^{56}Ni (Fassia et al. 2001) over the same period. This is illustrated in Fig. 13, where we compare the radioactive luminosity with the contemporary IR luminosity derived from the blackbody fits.

We can therefore immediately rule out radioactivity as the main source of the post-300 d IR energy. However, a much larger energy source is available. It is likely that of order 10^{51} ergs was stored in the kinetic energy of the ejecta, so it would take only ∼1% of this to account for the IR emission through the radiative heating of pre-existing (CSM) and/or newly-condensed (ejecta) dust. For example, for a progenitor with an extended structure or very dense wind, the ejecta/CSM interaction could rather easily convert ∼10% of the kinetic energy to radiation (Falk & Arnett 1977; Chugai et al. in preparation), thus providing the energy of the early light curve (0–40 days) which we know amounted to $\sim 10^{50}$ ergs (Fassia et al. 2000). If, then, a fraction (say 5–10%) of this early light curve emission were absorbed by CSM dust and re-emitted as an IR echo, it would account for the observed IR radiation. Gerardy et al.(2000) suggested that dust could be heated as a result of energy released in the ejecta/CSM interaction, either by direct shock-heating or by absorption of X-rays from the interaction region. However, they were not able to address the origin of the dust, i.e.

newly-formed in the SN ejecta or pre-existing in the CSM. As argued earlier, the large, low-temperature L'-band flux seen at 136 days must have been due to emission from pre-existing dust, i.e., an IR echo. However, such an argument is less convincing at the later times being considered here. The blackbody fits produce velocities not exceeding 4200 km s^{-1}, and generally slower than this (Table 8). Grain condensation in ejecta located at such velocities is conceivable. However, while the evolution of the line profiles provides convincing evidence that dust did condense in the ejecta, this does not automatically mean that this dust was also the source of the IR emission. IR radiation from a dusty CSM must therefore also be examined.

4.1.1 IR emission from pre-existing CSM dust

To try to distinguish between the IR echo and dust condensation scenarios, we consider first the possibility that the IR emission arose from pre-existing dust in the CSM. It is unlikely that CSM dust was directly heated by the supernova shock energy. The supernova radiation around maximum would have evaporated the dust to a radius r_v. The size of the dust-free cavity in such an explosion has been estimated by a number of authors to lie in the range 4,000–80,000 AU (Wright 1980; Bode & Evans 1980; Dwek, 1983, 1985; Graham & Meikle 1986; Gerardy et al. 2002). Dwek (1983, 1985) finds that for a supernova with a peak UV-optical bolometric luminosity of 1×10^{10} $L_\odot$ and an exponential decline rate timescale of 25 days, r_v is ∼4,000 AU for carbon-rich grains (T_{evap} = 1900 K) and 20,000 AU for oxygen-rich grains (T_{evap} = 1500 K). This is for 0.1 μm radius particles in an r^{-2} density distribution. The early bolometric light curve of SN 1998S derived from blackbody fits to the optical-IR photometry (Fassia et al. 2000) can be described as $L = 4.6{\times}10^{10} e^{-t/17.8d}$ $L_\odot$ erg s^{-1}. The more conservative spline-fit integration values yield $L = 1.5 \times 10^{10} e^{-t/24.4d}$ $L_\odot$ erg s^{-1}. Thus, given that $r_v \propto (L_{peak})^{0.5}$ (Dwek 1985) we conclude that the evaporation radius for SN 1998S would have been at least 5,000-9,000 AU for graphite grains, and at least 24,000-40,000 AU for silicate grains. The fastest moving ejecta material (∼10,000 km s^{-1}, Fassia et al. 2001) would have reached only 7,000 AU by the latest epoch (1242 d), almost certainly placing it well within the dust-free cavity throughout the observations presented here. The ejecta would, therefore, have been unable to interact directly with CSM dust.

It is likely that an X-ray precursor is produced as the forward shock moves through the dust-free low-density gas in the cavity. These X-rays would eventually reach the dust and hence may provide the energy needed for the IR emission. A concern might be that the X-rays could be severely attenuated by the gas in the cavity (assuming the unshocked gas in the cavity was not already fully ionized by the initial X-rays). Assuming a steady mass loss rate of $\sim 5 \times 10^{-4}$ M$_\odot$ yr^{-1} (see Section 1.1) we find that the gas column density between the shock front and the edge of the dust free cavity (assumed to be ∼25,000 AU) is 1.6×10^{-22}cm^{-1} at 333 d. This corresponds to an optical depth < 0.2 for X-rays of E$>$ 3 keV. Given the hard X-ray spectrum observed ($kT \approx 10$ keV, Pooley et al. 2002) we do not expect strong absorption of X-rays within the cavity. We note that X-rays would also be produced by the reverse shock. However, if it is radiative early on this might produce a CDS (Chevalier & Fransson 1985), causing additional attenuation of this X-ray component. The difficulty with the X-ray precursor scenario is that the observed X-ray luminosity is much less than that of the contemporary IR luminosity. At 674 days, measurements with Chandra indicate that $L_X = 10^{40}$ erg s^{-1} (Pooley et al. 2002), and as indicated above, we expect that these hard X-rays would only be weakly absorbed within the cavity. However, this luminosity is about ×15 lower than the blackbody-derived IR luminosity observed at this time. Light travel time effects mean that, in general, the observed IR emission would have been produced by the X-ray precursor at an earlier, possibly brighter phase. For example, by 664 d, a shock travelling at ∼10,000 km s^{-1} would have reached about 3800 AU. The largest delay would be for X-rays emitted directly away from us. This would amount to a delay of about 60 d for a 5,000 AU radius dust-free cavity to about 460 d for a 40,000 AU cavity. However, even a year later the IR luminosity has declined by only a factor of 3, i.e., it is still ×5 more luminous than the X-ray flux one year before. A perhaps rather desperate solution might be to suggest that more than ∼90% of the X-rays are being transformed into IR radiation, i.e., most of the X-rays are absorbed by the dust, yet leaving enough to be detected by Chandra. (We note the actual percentage could be somewhat less if the true X-ray temperature is higher than the ∼10 keV derived from the Chandra observations so that the X-ray flux was significant above Chandra's energy limit.) In such a scenario, we would expect the X-ray and IR light curves to be reasonably correlated. Between days 674 and 1044 the X-ray flux declined by about ×2 while the IR luminosity fell by ×3 in the same period. Given the complications of light travel times across the CSM, this might be consistent with an X-ray precursor-driven IR luminosity. However, a particular difficulty with the X-ray precursor model is that in general, for solid material, X-rays are more penetrating than UV/optical radiation (Wilms, Allen & McCray 2000). As indicated above, to account for the low X-ray/IR luminosity ratio we need the dust optical depth to the X-rays to be at least 2.5, in which case the optical depth to UV-optical photons would be even higher. Yet, for the IR-echo mechanism to produce the observed IR luminosity we require an optical depth to UV-optical-photons of about 0.2 (see below). In other words, in the case of the X-ray precursor mechanism, if we invoke sufficient dust absorption to account for the low X-ray/IR luminosity ratio then the IR-echo mechanism predicts an IR luminosity which exceeds the observed value by a large factor. Even if we adopt the lower $1.5 - 4.8$ μm luminosity values, a similar conclusion is reached. Gerardy et al. (2000) left open the possibility that the IR flux might arise from either direct shock heating or X-ray-precursor heating of pre-existing CSM dust. However, from the above discussion we believe that both possibilities are ruled out. Direct shock heating is impossible as the ejecta would not yet have reached the edge of the dust-free cavity. X-ray precursor heating is probably ruled out since it implies an IR-echo of much greater intensity than the observations could support.

We now consider thermal emission following the heating of CSM dust by supernova radiation emitted around the

time of maximum light, i.e., an "IR echo". Owing to the light travel time across the CSM, the IR emission seen at Earth at a given time originates from a zone bounded by ellipsoidal surfaces, with the axis coincident with the line-of-sight. The thickness of this zone is fixed by the characteristic width of the UV-optical light curve around maximum. While the UV-optical ellipsoid is still partially within the dust-free cavity, we expect the IR light curve to be relatively flat (Dwek 1983; Gerardy et al. 2002). However, once the whole ellipsoid has left the cavity, the IR flux declines. Even at our earliest epoch of 333 d, we see no sign of a plateau in the observed IR light curves, indicating that SN 1998S was already beyond the echo plateau phase. At 333 days the vertex of the ellipsoid would be 30,000 AU from the supernova. This indicates that, if the IR-echo scenario is valid, the cavity radius must have been less than 30,000 AU.

The flux, spectral energy distribution and evolution of a supernova/CSM IR-echo has been examined by a number of authors (Wright 1980; Bode & Evans 1980; Dwek, 1983, 1985; Graham & Meikle 1986; Gerardy et al. 2002). Of particular interest here is the study of SN 1979C by Dwek (1983). This supernova seems to have been similar to SN 1998S (cf. Liu et al. 2000). Both supernovae were unusually luminous at early times and both exhibited a strong IR excess at late times. Dwek (1983) argues that the late-time IR emission of SN 1979C was due to an IR-echo produced in a massive circumstellar wind. In addition, the early-time bolometric light curve adopted by Dwek (1983) for SN 1979C is exponential with a 23 day timescale - very similar to the spline-fit light curve for SN 1998S (see above and Fassia et al. 2000). The extinction towards SN 1979C was somewhat less than for SN 1998S, while their distances were almost identical. After correcting for the difference in extinction ($\Delta A_V \sim 0.25$), we find that the early-time bolometric light curve of SN 1998S (spline-fit) is $\times 1.3$ more luminous, while its post-300 d blackbody-derived IR luminosity is $\times 1.6$ less luminous than the corresponding values for SN 1979C. Scaling Dwek's results to SN 1998S indicates that about 20% of its early-time UV-optical output must have been absorbed by CSM dust. Applying Dwek's λ^{-1} emissivity model to a wind velocity of 40 km s^{-1} (Fassia et al. 2001), this yields a mass-loss rate of $1.1 \times 10^{-4} M_{\odot}$ yr^{-1}, comparable to the values indicated by optical, X-ray and radio studies (Anupama et al. 2001; Fassia et al. 2001; Pooley et al. 2002). Dwek's model parameters include an ISM gas-to-dust ratio of 160, a dust-free cavity radius of 20,000 AU, a steady mass-loss phase of 1.7 years, a grain radius of 0.1 μm and a grain material density of 3 g cm^{-3}. A longer mass-loss phase would result in only a modest decrease in the derived mass-loss rate.

The K and L-band IR-echo light curves of SN 1979C have been calculated by Bode & Evans (1980). At about 1 year, they find decline rates of 0.44 mag/100 d in K and 0.3 mag/100 d in L. Dwek finds an L-band decline rate of 0.4 mag/100 d for a putative galactic supernova once the plateau phase is over. Both authors assume r^{-2} CSM density laws. For SN 1998S, we observe decline rates of about 0.35 mag/100 d in K and 0.16 mag/100 d in L'. Similarly, for the total IR luminosity decline rate, while Dwek predicts an e-folding time of 340 days between years 1 and 2, our observations indicate e-folding times of about 470 days ($1-5$ μm luminosity) or 700 days (blackbody luminosity). However, these discrepancies may be indicative of a flatter CSM density law than r^{-2}, i.e. that the CSM wind was stronger in the past. In addition, these models assumed a spherically symmetric wind, whereas the SN 1998S CSM probably had a more flattened geometry (Leonard et al. 2000; Gerardy et al. 2000).

In addition to the modest decline rate disagreement, we also note that Dwek's model provides an imperfect match to the SN 1979C HKL SED. Similar discrepancies with the Dwek model are seen for the SN 1998S SEDs. Dwek argues that this may be due to the contamination of the H (and J) band fluxes with residual photospheric emission. However, our post-300 d IR spectra of SN 1998S do not support this explanation (cf. Fig. 11, day 333). We recall that the Dwek models utilise dust emissivity laws of λ^{-1} and λ^{-2}, whereas our analysis indicates that single temperature blackbodies yield a superior fit to the $HKL'M'$ SEDs of SN 1998S. This suggests that the dust grains are in an opaque clumped distribution, or are of larger individual size than in the Dwek model. Of course, the SED of the IR-echo model is made up of fluxes from material having a range of temperatures. It is therefore not clear that even with 'black-body' grains (or clumps) we would be able to reproduce the single temperature behaviour.

We conclude that the IR-echo scenario is not ruled out as providing the mechanism responsible for the post-300 d IR flux from SN 1998S. However, to make it work it has to be pushed to quite an extreme case where 20% of the early-time light is absorbed by the dust. There is little sign of such absorption in the form of reddening although, as already indicated, the dust grains could be clumped or are individually too large to give a reddening effect in the wavelength range studied. In addition, the simple spherically-symmetric IR-echo models do not fully agree with the observed decline rates and SEDs. Further progress will probably require more detailed IR-echo modelling, including asymmetric and episodic cases.

4.1.2 IR emission from newly-condensed ejecta dust

We now consider newly-condensed dust as the origin of the IR luminosity. Gerardy et al. (2000) suggested that the detailed shape and evolution of the Hα and He I profiles could be due to the ejecta impacting on a disk-shaped CSM, together with the condensation of dust within the ejecta. We agree that this is a promising scenario. As both Gerardy et al. (2000) and Leonard et al. (2000) point out, the relatively sudden fading of the central and red-shifted components of the H I, He I line profiles immediately suggests dust condensation in the ejecta, causing obscuration of the central and receding regions. A similar effect was observed in the ejecta line profiles of SN 1987A (Lucy et al. 1989; Spyromilio, Meikle & Allen 1990; Danziger et al. 1991) and, more recently, in the type IIP SN 1999em (Elmhamdi et al. 2003). The presence of CO emission from SN 1998S as early as 115 days (Fassia et al. 2001) lends credence to the dust condensation scenario. Moreover, in spite of the much

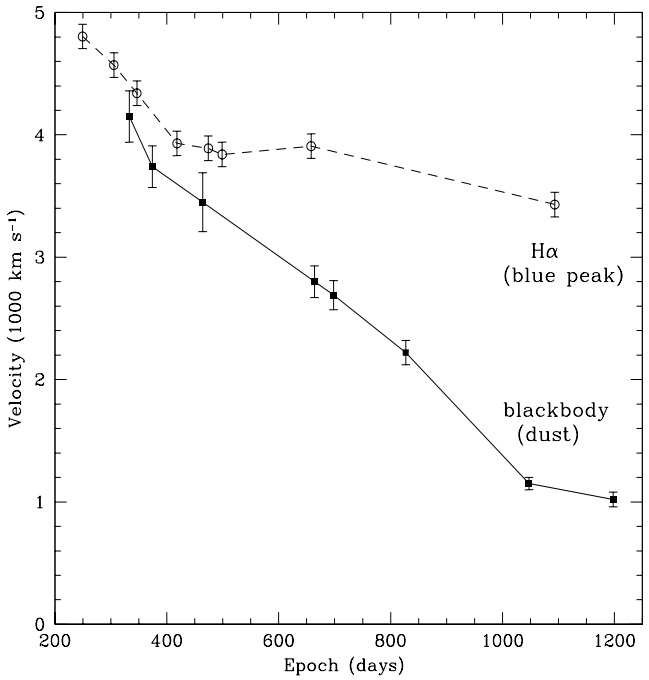

Figure 14. Comparison of velocity evolution of Hα blue peak (Table 6), and of blackbody from fit to IR SED (Table 8).

lower S/N of the He I 1.083 μm profile, plus its contamination by Pγ up to about the end of year 1, we judge that the obscuration effect is comparably strong at 0.66 μm and 1.08 μm, at least up to about day 400. This suggests that the dust became quickly optically thick either due to forming in clumps, or (less likely) growing rapidly to a large grain size. After day 400, the very low S/N of the He I red wing makes comparison impractical.

Could newly-condensed dust also have been responsible for the post-300 d IR luminosity of SN 1998S? As already indicated, there is an ample reservoir of energy available from the supernova kinetic energy which could radiatively heat the dust. For the pure blackbody fits, we note that in the period ∼330–400 days the velocity of the dust blackbody was ∼90% of the velocity of the blue-shifted H I, He I peaks (see Fig. 14). Consequently, for optically-thin dust characterised by λ^{-1}, λ^{-2} or λ^{+1} emissivities to account for the observed IR luminosity at this epoch, it would need to have condensed at velocities higher than those indicated by the blue peaks of the H and He lines, i.e. well beyond the main ejecta/CSM shock interaction. This seems unlikely. Moreover, as pointed out already, λ^{-1} and λ^{-2} emissivities yield poorer fits than does a pure blackbody. We therefore discount IR luminosity characterised by optically thin emissivities, and confine our attention to pure blackbody emission. After 333 d the dust and blue peak velocities decline roughly at the same rate until about 400 days after which the H I, He I peak velocity levelled off while that of the dust continued to decline. The near coincidence of the velocities for the ∼100 days after 333 d suggests a possible physical link between the origins of the H I, He I peaks and the IR luminosity. It has been recognised for many years (e.g., Chevalier & Fransson 1985) that the interaction of the supernova ejecta with a dense CSM will produce outer and reverse shocks. When radiative cooling is important at the reverse shock front, the gas undergoes a thermal instability, cooling to ∼10,000 K, thus forming a dense, relatively cool zone - the CDS. Line emission from low-ionisation species in the CDS will be produced (Chevalier & Fransson 1994). We suggest that this emission could have been responsible for the blue and red peaks of the Hα and He I line profiles. This leads to the interesting possibility that dust may have formed in the CDS at the ejecta/wind interface. (Note that this could be *as well as* dust formation in the metal-rich SN ejecta interior.) If cooling in the outer layer of the CDS, shielded from the reverse shock X-ray/UV radiation, brought the temperature to below the condensation temperature, dust could have formed and survived there. The physics here is reminiscent of the radiative shock of colliding winds of Wolf-Rayet stars, which is known to be a dust-forming site (Usov 1991). However, unlike the Wolf-Rayet material, the CDS has a normal composition with the carbon-to-oxygen ratio being less than unity. Consequently, at first sight, carbon dust might not be expected to form since all the carbon in the CDS would be bound into CO. However He^+ ions produced by X-ray absorption efficiently destroy CO via the reaction $He^+ + CO \rightarrow He + C^+ + O$ (Lepp, Dalgarno & McCray 1990), yielding the relatively low observed mass of CO (see Introduction). We estimate that dust formed in the CDS after day 200 may survive in the radiation field of SN 1998S. The occurrence of Rayleigh-Taylor or convective instabilities (Chevalier & Fransson 1994) can lead to the formation of opaque clumps of dust within the CDS, producing significant occultation of the central and receding parts of the supernova and radiative heating of the grains, while at the same time allowing some of the line radiation to escape from the approaching component of the CDS. (Given that the CDS has a temperature of ∼10,000 K, collisonal heating of the grains would be negligible, e.g. Dwek & Werner 1981). Thus, this scenario might simultaneously account for the strong IR flux, the obscuration effect and the blackbody velocity coincidence with that of the line profiles.

How much dust would be needed to achieve the required obscuration? Consider dust grains of radius a in spherical clumps of radius r_{cl}. For a spherical CDS whose thickness is small relative to its radius, the total mass of dust in clumps, M_{dust}, required to yield a CDS optical depth τ_{CDS} is given by $M_{dust} = (64/9)\pi^2 r_{CDS}^2 \tau_{CDS} n_g a^3 \rho r_{cl}/(1 - e^{-\tau_{cl}})$ where r_{CDS} is the radius of the CDS, n_g is the grain number density and ρ is the density of the dust grain material. τ_{cl} is the effective optical depth of a clump i.e. for a clump illuminated on one side, $e^{-\tau_{cl}}$ is the ratio of transmitted to incident fluxes, integrated over the projected area of the clump, and is given by $e^{-\tau_{cl}} = [1 - (1 + 2\tau_0)e^{-2\tau_0}]/2{\tau_0}^2$, where τ_0 is the centre to surface optical depth of a clump (e.g. Hobson & Padman 1993). If we assume that the grains are sufficiently large that their absorption cross-section at 5 μm equals their geometrical cross-section, i.e. $a > \lambda/2\pi \approx 1$ μm, then we may write $\tau_0 = \pi a^2 r_{cl}\, n_g$. Substituting into the equation for M_{dust}, we obtain $M_{dust} = (64/9)\pi r_{CDS}^2 \tau_{CDS} a \rho \tau_0/(1 - e^{-\tau_{cl}})$. For smaller grains (cf. Kozasa, Hasegawa & Nomoto 1989) if we assume that the ratio of absorption cross-section to geometrical cross section is proportional to λ^{-1}, then the dust mass becomes independent of a. For larger grains, the mass would increase in

proportion to the grain radius. At 346 d the radius of the Hα blue-peak emission region is 1.3×10^{16} cm. At this epoch the dust blackbody radius is 93% of this. If we assume that the dust and Hα emission zones are physically at about the same radius, then the smaller dust blackbody radius can be interpreted as a covering factor of about 86%, or $\tau_{CDS} \sim 2$. For near-opaque clumps, say $\tau_{cl} > 2$ ($\tau_0 > 1.8$), $a = 1$ μm, and a dust material density of 2.5 g cm^{-3} (a typical density of grain material), we obtain $M_{dust} > 2 \times 10^{-3}$ M$_\odot$. Note that this is a lower limit i.e. larger values of τ_{cl} yield higher masses. Repeating this calculation for subsequent epochs, we find that the dust mass (lower limit) remains roughly constant up to about 700 d, after which it declines. τ_{CDS} declines monotonically throughout this time, reaching 0.15 at 1000 d.

At 346 d the intensity ratio of the red and blue Hα peaks is 0.25. If we assume that the two peaks have the same intrinsic luminosity at all times, then we can interpret the red deficit as being due to an optical depth across the supernova of about 1.4. This is similar to the optical depth of 2 derived in the previous paragraph at the same epoch, using the velocities of the Hα peak and the IR blackbody. This lends support to the suggestion that condensing dust is responsible for both the line profile attenuation *and* the IR luminosity. A difficulty is that while the optical depths derived from the covering factor decrease with time, those derived from the Hα red/blue intensity ratio increase with time. A possible explanation might be that initially the optical depth was dominated by hot, newly-formed dust and it was purely this dust which was responsible for the obscuration *and* the observed near-IR flux. This would explain the similarity at 346 d of the optical depths derived in the two ways. However, if dust condensation was continuous throughout the 346–1093 d period it is possible that, if the dust which formed at earlier epochs cooled, our NIR observations would have detected a decreasing fraction of the total dust. Such a process would also mean that dust was present at an increasing range of temperatures, and this may account for the poorer blackbody fits at the later epochs. In summary, we agree about the plausibility of the dust-condensation scenario which Gerardy et al. (2000) put forward as one of a number of possibilities. We have refined this proposal in that we suggest that the dust is formed in the CDS, with the energy source for the IR emission coming ultimately from the shock interaction. However we note that if, as discussed in Section 4.1.1, the IR emission was predominantly due to an IR echo then the optical depth 'discrepancy' would disappear i.e. we would not then expect to see a correlation between the optical depths derived via the covering factor argument (which would be inappropriate for an IR echo) and those derived from the Hα red/blue intensity ratio.

4.2 Line profiles at 3 years

The Hα and He I 1.083 μm lines persisted beyond 3 years post-explosion (Figs. 8 & 9). At 1093 days the extreme blue wing of Hα was at a velocity of $\sim$5800 km s^{-1}, corresponding to 3650 AU, confirming that the CSM must have extended to at least this distance (for a CSM velocity of 40 km s^{-1}, this implies that the progenitor mass loss started at least 430 years prior to explosion). However, as explained above, even at this late epoch it is unlikely that the ejecta would have encountered any pre-existing CSM dust. The most notable change in the Hα profile is the appearance of an emission feature peaking at about the velocity of the supernova rest frame. Its wings extend to about $\pm$1000 km s^{-1} and so it cannot be due to the emergence of a spatially-coincident H II region as the supernova faded. It must be physically connected to the supernova. We note that the red side of the Hα feature is still very weak, presumably due to attenuation by dust which condensed in the SN. Thus, it is unlikely that we are witnessing emission from the central regions of the supernova. An alternative explanation is indicated by the 'clumpy wind' model of Chugai & Danziger (1994). In this scenario, we see emission from individual slow-moving CSM clumps as they are engulfed by the ejecta shock. As mentioned above, this was suggested by Gerardy et al. (2000) as an explanation for the earlier (and much stronger) central peak of the Hα feature. The increased prominence of the central feature by day 1093 could be partly due to a weakening of the direct interaction of the ejecta shock with the undisturbed, inter-clump CSM which is responsible for the blue peak. In the Introduction we pointed out that the early-time evolution of the [O III] 5007 Å CSM line indicated the existence of a denser CSM beginning at a radius of 2850 AU. This distance would have been reached by material moving at about 4500 km s^{-1} by 1093 days. We can see from Fig. 8 that at this epoch, a portion of the blue wing of the Hα line was moving at velocities exceeding this value. Thus, the Hα luminosity at 1093 days may have been enhanced by the interaction of the ejecta with a denser clumped CSM region.

The He I line is of much lower S/N and resolution. It peaks around –2000 km s^{-1} with the wings extending to ~ -5000 km s^{-1} and $\sim +3500$ km s^{-1}. We find that by removing the rest frame velocity component from the Hα profile and then degrading its resolution to that of the He I line, a reasonable match between the two profiles is obtained. We conclude that, if present, a rest frame zero velocity component was much weaker in the He I 1.083 μm line.

4.3 $(K - L')_0$ colour and the origin of dust associated with supernovae

The work described above demonstrates the value of late-time observations at wavelengths longer than the K-band for constraining the conditions under which dust is present in or near supernovae. Unfortunately, the only other SN for which such a comprehensive data set is available is SN 1987A (Bouchet & Danziger 1993 and references therein; Caldwell et al. 1993 and references therein). Indeed, besides SNe 1987A and 1998S, there are only four other SNe for which any L or L' observations beyond 100 days are available viz. SNe 1979C (IIL) (Merrill 1980, private communication), 1980K (IIL) (Dwek et al. 1983), 1993J (IIb) (Matthews et al. 2002) and 2002hh (IIp) (Pozzo et al., in preparation). In Fig. 15, we show the dereddened colour, $(K - L')_0$, versus time for the 6 SNe. For SNe 1979C and 1980K, L-band rather than L'-band magnitudes were available. In addition the L'-band used for the SN 1993J observations is centred at a somewhat shorter wavelength (3.68 μm)

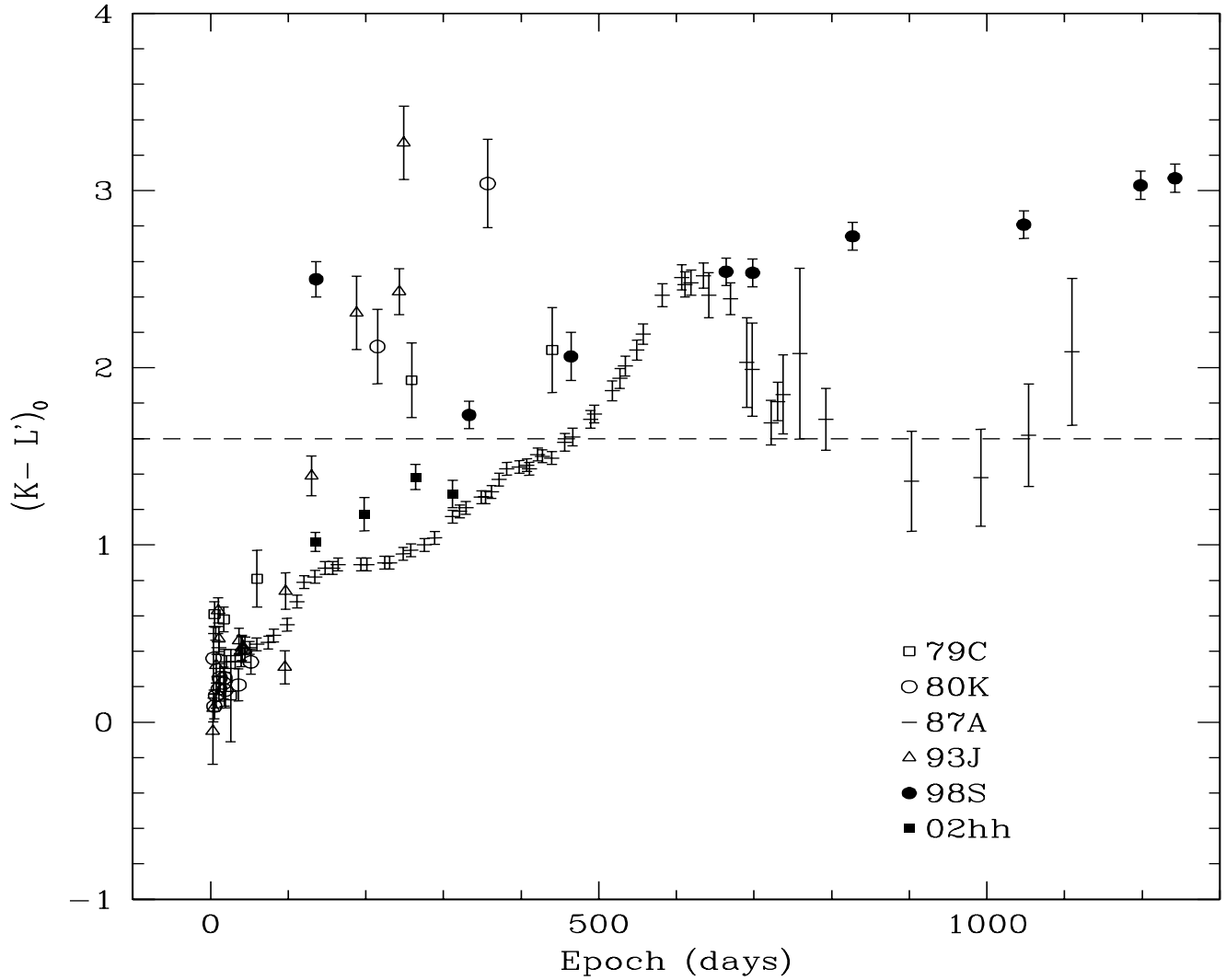

Figure 15. Evolution of the extinction-corrected colour $(K - L')_0$ for six core-collapse supernovae. The epoch gives the approximate number of days since outburst. We suggest that a value of $(K - L')_0 > 1.6$ (i.e. above the dashed horizontal line) indicates evidence of IR emission from dust (see text).

than the more typical value of around 3.8 μm. These magnitudes were therefore converted to L' (3.8 μm) as described in Appendix A. In addition, the colours have been corrected for extinction using the Cardelli et al. (1989) law (see Appendix B). For SNe 1998S and 1993J, the epochs are with respect to outburst. For the others, the fiducial time is BV maximum. However, the time from explosion to maximum is probably at most 15–25 days, and so has a negligible effect on the conclusions reached below since they are based on late-time observations. For all six SNe, we see (Fig. 15) that up to day 100, $(K - L')_0$ lies in the range 0.0–0.8, with a slight trend toward redder values with time. Beyond this epoch, the $(K - L')_0$ colour continues to redden, sometimes dramatically so. For blackbody emission, and a conservative maximum dust temperature of 1300 K, $(K - L')_0 = 1.6$. Moreover, we know that for SNe 1987A and 1998S, when an IR continuum rising to longer wavelengths was present, $(K - L')_0$ was also in excess of 1.6. It therefore seems reasonable to take $(K - L')_0 > 1.6$ as evidence of IR emission from dust, via an IR-echo and/or from newly-condensing dust. In Fig. 15, $(K - L')_0$ values as high as $\sim$3 are seen, corresponding to a blackbody temperature as low as 800 K.

During the 100–350 day era, while SNe 1987A and 2002hh showed a gradual increase in $(K - L')_0$, the values for SNe 1979C, 1980K, 1993J and 1998S jumped to $(K - L')_0 >\sim 2.0$. The different behaviour of SNe 1987A and 2002hh on the one hand and the other 4 SNe on the other, suggests IR emission was taking place under somewhat different physical conditions in these two groups of SNe. A clue to the origin of this difference is provided by observations which show that SNe 1979C, 1980K, 1993J and 1998S were surrounded by large amounts of circumstellar material (SN 1979C - Panagia et al. 1980; Fransson et al. 1984; Fesen et al. 1999. SN 1980K - Leibundgut et al. 1991; Fesen et al. 1999. SN 1993J - Garnavich & Ann

1994; Patat, Chugai & Mazzali 1995; Matheson et al. 2000a, 2000b. SN 1998S - Leonard et al. 2000; Gerardy et al. 2000; Fassia et al. 2001). In contrast, the wind density of the SN 1987A progenitor was very low in its final blue supergiant phase ($< 1 \times 10^{-8} M_{\odot} yr^{-1}$ for 500 km s^{-1}, Lundqvist 1999) and its red supergiant wind with $< 5 \times 10^{-5} M_{\odot} yr^{-1}$ (e.g., Blondin & Lundqvist 1993) is too far from the supernova to cause early CSM interaction. Up to day 389 SN 2002hh also shows little evidence of strong CSM interaction in its spectra (Pozzo et al., in preparation). We therefore suggest that supernovae which show $(K - L')_0 > 1.6$ during 100–350 days post-explosion, probably have massive circumstellar winds in their immediate vicinity.

The precise origin of the strong IR excess [$(K - L')_0 > 1.6$] in the 100–350 d period is not straightforward to determine. As we have already indicated, for SN 1998S at 136 d it is unlikely that the IR emission is due to condensing dust since the required IR luminosity and the red $(K-L')_0$ colour would require the emitting dust to be lying at a velocity of ∼67,000 km s^{-1}. A similar, though somewhat weaker, point can be made for SN 1993J at 130 d where, following correction for photospheric emission (Matthews et al. 2002) the blackbody temperature would be ∼800 K and the blackbody velocity around 8000 km s^{-1}. However, the situation is less clear for the other examples of high $(K - L')_0$ in this era. The exceptionally high late-time IR luminosity for SN 1979C poses a particularly difficult challenge. For a blackbody to yield its L' flux and colour on day 259 it would have to be expanding at 10,000 km s^{-1}. This seems to argue against an ejecta dust origin, although we note the 223 d Hα profile of SN 1979C also indicates a shock velocity of about 10,000 km s^{-1} (Filippenko 1997). Yet to account for the IR emission with the IR-echo model, it has to be pushed to an extreme case where around 30% of its early-time UV-optical output must have been absorbed by CSM dust (Dwek 1983). It may be, therefore that emission from both a CDS and an IR-echo have to be invoked to account for the total IR emission from SN 1979C. For SN 1998S there must also have been a period around 200–300 days when the contributions from both sources were comparable. Given that SNe 1980K and 1993J also possessed massive CSMs, we suggest that the IR excess in these cases may also have been a mixture of emission from CDS dust and CSM dust. By ∼500 d we know that dust condensing and cooling in the ejecta of SN 1987A was almost certainly responsible for the reddening of the $(K - L')_0$ colour (e.g. Wooden 1989; Bouchet & Danziger 1993; Meikle et al. 1993; Roche et al. 1993; Wooden et al. 1993). From the discussion above we also favour dust condensation in SN 1998S as the explanation for its IR luminosity after ∼1 year. Given the similarity of SN 1979C to 1998S, we suggest that its day 440 $(K - L')_0$ point also indicates that most of its IR emission was from CDS dust at this time. We note that at this phase the blackbody velocity of SN 1979C would be only about 3000 km s^{-1}.

We therefore propose that the appearance of a strong $(K - L')_0$ excess during the first year is indicative of a massive CSM. The IR flux can be a mixture of emission from CDS dust and an IR-echo. Determination of the relative contributions requires good late-time IR and optical coverage, as this paper has shown. For the progenitors of SNe which do not show an IR-excess in the 100–350 day period (e.g., SNe 1987A, 2002hh), it is much less likely that they were surrounded by a massive CSM in their immediate vicinity. If such SNe subsequently produce an IR excess this is probably due to dust condensation throughout the ejecta as was inferred for SN 1987A.

5 CONCLUSIONS

We have presented post-300 d infrared and optical observations of the SN IIn 1998S which extend to longer wavelengths and later epochs than has ever been achieved for this type of supernova. SN 1998S is only the second ever supernova for which M'-band has been detected. The IR photometry presented here, together with an earlier measurement by Fassia et al. (2000), has revealed a strong IR-excess during the period 136 to 1242 days. Spectroscopy in the HK bands show a continuum rising towards longer wavelengths. Broad Hα and He I 1.083 μm line profiles present at ∼4 months had undergone a dramatic change when they were recovered by Gerardy et al. (2000) at about 8 months. By this time, both lines took the form of a triple peak structure with a central peak close to the supernova rest frame velocity, and with the two other peaks lying at –4860 km s^{-1} and +3400 km s^{-1} respectively. Gerardy et al. argue that this could be indicative of emission from a disk-like or ring-like CSM. Our observations show that as the supernova evolved, the redward half of the profiles became increasingly weak relative to the blue part so that by the end of the second year the red side had almost completely vanished. We agree with Gerardy et al. (2000) and Leonard et al. (2000) that this is strongly indicative of dust condensation within the ejecta of the supernova. The change in the appearance of the Hα profile by 1093 d together with the early-time evolution of the narrow CSM [O III] 5007 Å line may indicate a density discontinuity at about 2850 AU implying that the progenitor mass-loss rate underwent a decline about 340 years ago. The velocity of the extreme blue wing of the Hα line at 1093 days implies that the CSM extended to at least 3650 AU indicating that mass loss had been taking place for at least 430 years prior to explosion.

The intensity and rise of the HK continuum towards longer wavelengths together with the relatively bright L' and M' magnitudes suggests strongly that the IR emission was due to hot dust condensing in the ejecta and/or pre-existing in the CSM. We find that the SED represented by the $HKL'M'$ magnitudes and by the HK continua (when available) can be well-reproduced with single-temperature blackbody functions having temperatures of about 1250 K at 333 days declining to about 1100 K at 464 days. Subsequent epochs yield temperatures declining to about 900 K at 3 years, although the fits are somewhat poorer. This probably indicates an increasing range of temperatures in the emission regions. Fits achieved with blackbodies weighted with a λ^{-1} or λ^{-2} emissivity are almost always less successful than those yielded by pure blackbodies. Newly-condensed iron whiskers having a λ^{+1} emissivity also seem unlikely as they would have to form beyond the CDS. We conclude that the IR emission arises from dust in the form of IR-opaque

clumps or having a large ($a > 1\mu$m) grain size.

We have considered possible origins for the strong, post-300 d IR emission. A significant amount of direct heating of condensed ejecta dust by ongoing radioactive decay is ruled out since the observed IR emission exceeds the radioactive luminosity by a substantial factor. We also rule out the possibility of direct heating of pre-existing CSM dust by the shock, since it would not have reached the edge of the dust-free cavity. X-ray precursor heating of CSM dust is also ruled out since it would imply the additional presence of an IR-echo of much greater luminosity than the observations could support.

We are therefore left with the IR-echo and condensing dust hypotheses. In favour of the IR-echo explanation, Dwek's (1983) model with a λ^{-1} dust emissivity suggests that the observed IR luminosity could be produced by a slow wind of $\sim 10^{-4}$M$_\odot$ yr^{-1} which is similar to that indicated by optical, X-ray and radio observations of SN 1998S. This assumes the typical ISM gas-to-dust ratio of 160 in the progenitor CSM. In addition, if we adopt a λ^{-1} emissivity law, then condensing dust would be unable to supply sufficient IR luminosity. However, our measurements tend to disfavour SEDs weighted with a λ^{-1} or λ^{-2} emissivity. Moreover, for the IR-echo scenario to work for SN 1998S at $t > 300$ d, we must invoke a rather extreme case where at least 20% of the UV-optical luminosity is absorbed by the CSM dust. In addition, against the IR-echo scenario is the disagreement in the observed and predicted decline rates and SEDs, although it may be possible to eliminate these discrepancies through more detailed IR-echo modelling, including asymmetric and episodic cases. We therefore do not rule out the IR-echo scenario. At the earlier epoch of 136 d, an IR-echo seems to be the only plausible explanation for the IR luminosity.

In favour of the condensing dust hypothesis is the success of the single temperature pure blackbody fits at about 1 year. Dust condensing in optically thick clumps within a physically relatively thin shell symmetrical about the supernova centre-of mass might be expected to exhibit such temperature uniformity. (Light travel time effects would be negligible in this case since even at 2 years the ejecta radius would only be about 10 light days.) Moreover, the coincidence at about 1 year of the blue-peak velocities of the Hα and He I 1.083 μm lines with that derived from the blackbody fits to the IR magnitudes suggests a physical connection. This is supported by the similar values at about 1 year for the optical depths derived from the Hα line profile, the He I 1.083 μm line profile, and that obtained from the blackbody-derived dust covering fraction. We suggest that this connection is the CDS formed as a result of the ejecta-CSM interaction. It is possible that conditions in the CDS would allow the condensation of dust. Moreover the highest blackbody temperature we derive is 1250 K, which is also believed to be compatible with grain condensation, though only slightly higher temperatures may not be (Gehrz 1988). Assuming that all the dust at about 1 year is at the same temperature, we estimate that as early as 1 year, over 10^{-3} M$_\odot$ had formed. The apparent decrease in the dust mass after about 700 d together with the reduced success of the blackbody fits to the IR SED may indicate that dust condensation was actually still ongoing but that an increasing proportion had cooled to temperatures where the bulk of the flux was emitted beyond NIR wavelengths. Given these arguments, we tend to favour dust condensation as the origin of *both* the post-300 d IR luminosity and the line profile attenuation.

It should be stressed that in the dust condensation scenario, the total dust mass produced could be very much larger than the $\sim \times 10^{-3}$ M$_\odot$ lower limit. Most of the dust could have been invisible due to the clump opacities being much higher than that necessary to produce a blackbody spectrum, and increasingly large amounts could have gone undetected due to the cooling of an increasingly large proportion of the dust beyond the reach of the NIR observations. The possibility of very opaque clouds is also raised by Elmhamdi et al. (2003), who obtain a somewhat weaker lower limit of $\sim 10^{-4}$ M$_\odot$ of dust for the type IIP SN 1999em based on the evolution of the [O I] 6300 Å profile. In addition, our proposal that dust formed in the CDS does not exclude the possibility that dust also condensed deep within in the metal-rich SN ejecta interior. Indeed the presence of a CO emission zone on day 115 at a velocity of only 2200 km s^{-1} (Fassia et al. 2001) suggests that a cool dust-forming environment deep in the ejecta might have developed. Our dust mass lower limit for SN 1998S is consistent with the $\sim$0.1–0.3 M$_\odot$ of condensed dust in SN 1987A deduced from metal depletion (Lucy et al. 1991; Dwek et al. 1992; Spyromilio & Graham 1992). However, SN 1987A was peculiar. Moreover, SNe IIn make up only 10–15% of all type II events (Cappellaro & Turatto 2001). Of the three CCSNe (87A, 98S, 99em), only SN 1999em may be described as 'typical', but it is only one event. It is therefore premature to conclude that high rates of dust condensation occur in all type II events. Consequently, the exact significance of SNe II for cosmic dust production is undecided. For further progress to be made, studies such as presented here should be carried out for a statistically significant sample of supernovae, and extended to even longer IR wavelengths.

Comparison of the $(K - L')_0$ evolution for a number of type II SNe, suggests that this may be a useful tool for discriminating between supernovae whose progenitors possessed or lacked a massive CSM. We propose that the appearance of a strong $(K - L')_0$ excess $[(K - L')_0 > 1.6]$ during the first year is indicative of a massive CSM. The IR flux at this time can be a mixture of emission from CDS dust and an IR-echo i.e., two populations of dust may exist. The newly-formed ejecta dust would be responsible for the attenuation of the red sides of the line profiles. Determination of the relative contributions by the two populations to the IR flux requires good wavelength coverage at late-times, extending as far as the L' and M' bands or even further to the mid-IR. For the progenitors of SNe which do not show an IR-excess in the 100–350 day period (e.g., SNe 1987A, 2002hh), it is much less likely that they were surrounded by a massive CSM in their immediate vicinity. If such SNe subsequently produce an IR excess this is probably due to dust condensation throughout the ejecta as was inferred for SN 1987A.

ACKNOWLEDGEMENTS

We thank T. Dahlén, D. Farrah, D. Folha, P. Hirst, S. Leggett and D. Lennon for carrying out some of the observations presented here. We are also grateful to R. Fesen, A. Filippenko, C. Gerardy, D. Leonard and T. Matheson for providing their spectra in digitised format. We also thank D. Leonard and T. Matheson for the use of their unpublished spectrum of 1999 December 15. We thank L. Lucy for helpful discussions. This work is based on observations collected at the Isaac Newton Telescope (INT), La Palma, the Nordic Optical Telescope (NOT), La Palma and the United Kingdom Infrared Telescope (UKIRT), Hawaii. The INT is operated on the island of La Palma by the Isaac Newton Group (ING) in the Spanish Observatorio del Roque de los Muchachos of the Instituto de Astrofisica de Canarias. The NOT is operated on the island of La Palma jointly by Denmark, Finland, Iceland, Norway, and Sweden, in the Spanish Observatorio del Roque de los Muchachos of the Instituto de Astrofisica de Canarias. UKIRT is operated by the Joint Astronomy Centre on behalf of the U.K. Particle Physics and Astronomy Research Council. Some of the data reported here were obtained as part of the ING and UKIRT Service Programmes. MP is supported through PPARC grant PPA/G/S/2001/00512. PL and NNC are grateful for support from the Royal Swedish Academy of Sciences.

REFERENCES

Anupama G.C., Sivarani T., Pandey G., 2001, A&A, 367, 506
Aspin C., 1996, Starlink User Note 41.0
Bersanelli M., Bouchet P., Falomo R., 1991, A&A, 252, 854
Blondin J.M., Lundqvist P., 1993, ApJ, 405, 337
Bode M.F., Evans A., 1980, MNRAS, 193, 21
Bouchet P., Danziger I.J., 1993, A&A, 273, 451
Bowen D.V., Roth K.C., Meyer D.M., Blades J.C., 2000, ApJ, 536, 225
Burstein D., Heiles C., 1982, AJ, 87, 1165
Caldwell J.A.R. et al., 1993, MNRAS, 262, 313
Cappellaro E., Turatto M., 2001, in The influence of binaries on stellar population studies, Dordrecht: Kluwer Academic Publishers, 2001, xix, p. 582
Cardelli J.A., Clayton G.C., Mathis J.S., 1989, ApJ, 345, 245
Catchpole R., Glass I., 1987, IAU Circ. 4457
Cernuschi F., Marsicano F.R., Kimel I., 1965, Ann. d'Astr., 28, 860
Cernuschi F., Marsicano F., Codina S., 1967, Ann. d'Astr., 30, 1039
Chevalier R.A., Fransson C., 1985, in Supernovae as distance indicators; Proceedings of the Workshop, Cambridge, MA, September 27-28, 1984. Berlin and New York, Springer-Verlag, 1985, p. 123.
Chevalier R.A., Fransson C., 1994, ApJ, 420, 268
Chugai N.N., 2001, MNRAS, 326, 1448
Chugai N.N., Danziger I.J., 1994, MNRAS, 268, 173
Chugai N.N., Blinnikov S.I., Fassia A., Lundqvist P., Meikle W.P.S., Sorokina E.I., 2002, MNRAS, 330, 473
Clocchiatti A., Wheeler J.C., Barker E.S., Filippenko A.V., Matheson T., Liebert J.W., 1995, ApJ, 446, 167
Colgan S.W.J., Haas M.R., Erickson E.F., Lord S.D., Hollenbach D.J., 1994, ApJ, 427, 874
Danziger I.J., Lucy L.B., Bouchet P., Guiffes C., 1991, in Woosley S.E., ed., Supernovae. Springer-Verlag, New York, p.69
de Vaucouleurs G., de Vaucouleurs A., Buta R., Ables H.D., Hewitt A.V., 1981, PASP, 93, 36
Draper P.W., Gray N., Berry D.S., 2002, Starlink User Note 214.10
Dunne L., Eales S., Ivison R., Morgan H., Edmunds M., 2003, Nat, 424, 285
Dwek E., Werner M.W., 1981, ApJ, 249, 138
Dwek E., 1983, ApJ, 274, 175
Dwek E., 1985, ApJ, 297, 719
Dwek E., 1991, in Supernovae. The Tenth Santa Cruz Workshop in Astronomy and Astrophysics, July 9-21, 1989, Lick Observatory. S.E. Woosley editor, Springer-Verlag, New York, p. 54
Dwek E., 1998, ApJ, 501, 643
Dwek E., 2004, ApJ, in press; 2004, preprint (astro-ph/0401074).
Dwek E. et al., 1983, ApJ, 274, 168
Dwek E., Moseley S.H., Glaccum W., Graham J.R., Loewenstein R.F., Silverberg R.F., Smith R.K., 1992, ApJ, 389, L21
Economou F., Jenness T., Currie M., Adamson A., Allan A., Cavanagh B., 2003, Starlink User Note 230.5.
Elmhamdi A. et al., 2003, MNRAS, 338, 939
Falk S.W., Arnett W.D., 1977, ApJS, 33, 515
Fassia A. et al., 2000, MNRAS, 318, 1093
Fassia A. et al., 2001, MNRAS, 325, 907
Fesen R.A. et al., 1999, AJ, 117, 725
Filippenko A.V., 1997, ARA&A, 35, 309
Filippenko A.V., Moran E.C., 1998, IAU Circ. 6830
Fransson C., Benvenuti P., Wamsteker W., Gordon C., Hempe K., Reimers D., Palumbo G.G.C., Panagia N., 1984, A&A, 132, 1
Garnavich P.M., Ann H.B., 1994, AJ, 108, 1002
Garnavich P., Challis P., Kirshner R., 1998, IAU Circ. 7047
Gehrz R.D., 1988, ARA&A, 26, 377
Gehrz R., 1989, in Interstellar Dust: Proceedings of the 135th Symposium of the International Astronomical Union, 26-30 July, 1988, Santa Clara, California. L.J. Allamandola and A.G.G.M. Tielens editors, Kluwer Academic Publishers, Dordrecht, p. 445
Gerardy C.L., Fesen R.A., Höflich P., Wheeler J.C., 2000, AJ, 119, 2968
Gerardy C.L. et al., 2002, ApJ, 575, 1007
Graham J.R., Meikle W.P.S., 1986, MNRAS, 221, 789
Grasberg E.K., Imshennik V.S., Nadyozhin D.K., 1971, Ap& SS, 10, 28
Gruendl R.A., Chu Y.H., Van Dyk S.D., Stockdale C.J., 2002, AJ, 123, 2847
Hamuy M., 2003, in Core Collapse of Massive Stars, ed. C.L. Fryer, Kluwer, Dordrecht.
Hobson M.P. and Padman R., 1993, MNRAS, 264, 161
Hoyle F., Wickramasinghe N.C., 1970, Nat, 226, 62
Hoyle F., Wickramasinghe N.C., 1999, Ap&SS, 268, 77
Leibundgut B., Kirshner R.P., Pinto P.A., Rupen M.P., Smith R.C., Gunn J.E., Schneider D.P., 1991, ApJ, 372, 531
Kozasa T., Hasegawa H., Nomoto K., 1989, ApJ, 344, 325
Lentz E.J. et al., 2001, ApJ, 547, 406
Leonard D.C., Filippenko A.V., Barth A.J., Matheson T., 2000, ApJ, 536, 239
Lepp S., Dalgarno A., McCray R., 1990, ApJ, 358, 262
Li C., Wan Z., 1998, IAU Circ. 6829
Li H., McCray R., Sunyaev R.A., 1993, ApJ, 419, 824
Li W., Filippenko A.V., Van Dyk S.D., Hu J., Qiu Y., Modjaz M., Leonard D.C., 2002, PASP, 114, 403
Liu Q.-Z., Hu J.-Y., Hang H.-R., Qiu Y.-L., Zhu Z.-X., Qiao Q.-Y., 2000, A&ASS, 144, 219
Lucy L.B., Danziger I.J., Gouiffes C., Bouchet P., 1989, in Tenorio-Tagle G., Moles M., Melnick J., eds, IAU Colloq. 120, Structure and Dynamics of the Interstellar Medium. Springer-Verlag, New York, p. 164
Lucy L.B., Danziger I.J., Gouiffes C., 1991, in Supernovae. The Tenth Santa Cruz Workshop in Astronomy and Astro-

physics, July 9-21, 1989, Lick Observatory. S.E. Woosley editor, Springer-Verlag, New York, p. 82
Lundqvist P., 1999, ApJ, 511, 389
Lundqvist P., Fransson C., 1988, A&A, 192, 221
McGregor P.J., Hyland, 1987, IAU Circ. 4468
Matheson T. et al., 2000a, AJ, 120, 1487
Matheson T., Filippenko A.V., Ho L.C., Barth A.J., Leonard D.C., 2000b, AJ, 120, 1499
Matthews K., Neugebauer G., Armus L., Soifer B.T., 2002, AJ, 123, 753
Meikle W.P.S., Spyromilio J., Allen D.A., Varani G.-F., Cumming R.J., 1993, MNRAS, 261, 535
Meikle P., Mattila S., Smartt S., MacDonald E., Clewley L., Dalton G., 2002, IAU Circ. 8024
Meikle P., Fassia A., Geballe T.R., Lundqvist P., Chugai N., Farrah D., Sollerman J., 2003, in From Twilight to Highlight: The Physics of Supernovae, Proceedings of the ESO/MPA/MPE Workshop, Garching, Germany, 29-31 July 2002, p.229
Merline W.J., Howell S.B., 1995, Exp. Astron., 6, 163
Morgan H.L., Dunne L., Eales S.A., Ivison R.J., Edmunds M.G., 2003, ApJ, 597, L33
Morrison P., Sartori L., 1969, ApJ, 158, 541
Moseley S.H., Dwek E., Glaccum W., Graham J.R., Loewenstein R.F., Silverberg R.F., 1989, Nat, 340, 697
Nozawa T., Kozasa T., Umeda H., Maeda K., Nomoto K., 2003, ApJ, 598, 785
Panagia N. et al., 1980, MNRAS, 192, 861
Patat F., Chugai N., Mazzali P.A., 1995, A&A, 299, 715
Pooley D. et al., 2002, ApJ, 572, 932
Roche P.F., Aitken D.K., Smith C.H., 1993, MNRAS, 261, 522
Romaniello M., Panagia N., Scuderi S., Kirshner R.P., 2002, AJ, 123, 915
Roscherr B., Schaefer B.E., 2000, ApJ, 532, 415
Sanders R.H., Verheijen M.A.W., 1998, ApJ, 503, 97
Schlegel E.M., 1990, MNRAS, 244, 269
Shortridge K., 1991, FIGARO General Data Reduction and Analysis Starlink MUD, RAL, June 1991.
Spyromilio J., Graham J.R., 1992, MNRAS, 255, 671
Spyromilio J., Leibundgut B., 1996, MNRAS, 283, L89
Spyromilio J., Meikle W.P.S., Learner R.C.M., Allen D.A., 1988, Nat, 334, 327
Spyromilio J., Meikle W.P.S., Allen D.A., 1990, MNRAS, 242, 669
Spyromilio J., Stathakis R.A., Cannon R.D., Waterman L., Couch W.J., 1991, MNRAS, 248, 465
Spyromilio J., Leibundgut B., Gilmozzi R., 2001, A&A, 376, 188
Suntzeff N.B., Bouchet P., 1990, AJ, 99, 650
Tielens A.G.G.M., 1990, in Submillimitre Astronomy; Watt G.D., Webster A.S., eds. Dordrecht, Kluwer, p.13.
Timmes F.X., Woosley S.E., Hartmann D.H., Hoffman R.D., 1996, ApJ, 464, 332
Todini P., Ferrara A., 2001, MNRAS, 325, 726
Tokunaga A.T., Simons D.A., Vacca W.D., 2002, PASP, 114, 180
Tully R.B., 1988, Nearby Galaxies Catalog (New York: Cambridge University Press)
Usov V.V., 1991, MNRAS, 252, 49
Wang L., Howell D.A., Höflich P., Wheeler J.C., 2001, ApJ, 550, 1030
Whitelock P.A. et al., 1989, MNRAS, 240, 7
Wickramasinghe N.C., 1992, Ap&SS, 198, 161
Wilms J., Allen A., McCray R., 2000, ApJ, 542, 914
Wooden D.H., 1989, PhD Thesis California University, Santa Cruz
Wooden D.H., Rank D.M., Bregman J.D., Witteborn F.C., Tielens A.G.G.M., Cohen M., Pinto P.A., Axelrod T.S., 1993, ApJS, 88, 477
Woosley S.E., Weaver T.A. 1995, ApJS, 101, 181
Wright E.L., 1980, ApJ, 242, L23

Table A1. E($K - L'$) values for the type II SNe plotted in Fig. 15.

SN	E($B - V$)	E($K - L'$)
1979C	0.18[a]	0.04
1980K	0.4[b]	0.08
1987A	0.2[c]	0.04
1993J	0.24[d]	0.05
1998S	0.22[e]	0.05
2002hh	$\sim$2.0[f]	$\sim$0.48

[a] de Vaucouleurs et al. 1981.
[b] Burstein & Heiles 1982.
[c] Romaniello et al. 2002.
[d] Clocchiatti et al. 1995.
[e] Fassia et al. 2000.
[f] Meikle et al. 2002

APPENDIX A: CONVERSION OF $K - L$ TO $K - L'$ COLOUR

For SNe 1979C and 1980K, L-band rather than L'-band magnitudes were available. In addition the L'-band used for the SN 1993J observations is centred at a somewhat shorter wavelength (3.68 μm) than the more typical value of around 3.8 μm. We therefore converted these magnitudes to L'(3.8 μm), based on the colours, spectra and dust temperatures derived for SN 1998S around the same period. We adopted $K - L'(3.8\ \mu\mathrm{m}) = K - L(3.5\ \mu\mathrm{m}) + 0.3$ for SNe 1979C and 1980K, and $K - L'(3.8\ \mu\mathrm{m}) = K - L'(3.68\ \mu\mathrm{m}) + 0.12$ for SN 1993J. At epochs earlier than 100 days, when the spectra are photosphere-dominated, the differences between $K - L$ and $K - L'$ are small and so no corrections were made.

APPENDIX B: EXTINCTION CORRECTION FOR THE $K - L'$ COLOUR.

Prior to plotting the $(K - L')_0$ colour evolution in Fig. 15, correction for extinction was applied using $\mathrm{E}(K - L') = 0.211\ \mathrm{E}(B - V)$, derived from the interstellar extinction law of Cardelli et al. (1989). These corrections are listed in Table B1. Apart from the case of SN 2002hh, the corrections are small.

This paper has been produced using the Royal Astronomical Society/Blackwell Science LaTeX style file.